



โครงการการเรียนการสอนเพื่อเสริมประสบการณ์

กลไกการเกิดแผ่นดินไหวตามเขตมุดตัวของเปลือกโลก
กลุ่มหมู่เกาะอินโดนีเซีย

โดย

นางสาวพัชราพร เพ็ชรดี

เลขประจำตัวนิตินิติ 5732740023

โครงการนี้เป็นส่วนหนึ่งของการศึกษาระดับปริญญาตรี
ภาควิชาธรณีวิทยา คณะวิทยาศาสตร์ จุฬาลงกรณ์มหาวิทยาลัย

ปีการศึกษา 2560

บทคัดย่อและฉบับเต็มของงานวิจัยของโครงการที่ให้บริการในคลังปัญญาจุฬาฯ (CUIR)

เป็นเพียงข้อมูลของนิตินิติเจ้าของโครงการทางวิชาการที่ส่งผ่านทางคณะที่สังกัด

The abstract and full text of senior projects in Chulalongkorn University Intellectual Repository (CUIR)

are the senior project authors' files submitted through the faculty.

กลไกการเกิดแผ่นดินไหวตามเขตมุดตัวของเปลือกโลก กลุ่มหมู่เกาะอินโดนีเซีย

นางสาวพัชรพร เพ็ชรดี

โครงการนี้เป็นส่วนหนึ่งของการศึกษาตามหลักสูตรปริญญาวิทยาศาสตรบัณฑิต
ภาควิชาธรณีวิทยา คณะวิทยาศาสตร์ จุฬาลงกรณ์มหาวิทยาลัย
ปีการศึกษา 2560

FOCAL MECHANISM ALONG THE SUBDUCTION ZONE, INDONESIAN
ARCHIPELAGO

Miss Patcharaporn Petchdee

A Project submitted in Partial Fulfillment of the Requirements
for the Degree of the Bachelor of Science Program in Geology
Department of Geology, Faculty of Science, Chulalongkorn University
Academic Year 2017

Project Title: FOCAL MECHANISM ALONG THE SUBDUCTION ZONE, INDONESIAN
ARCHIPELAGO

By: Miss Patcharaporn Petchdee

Department: Geology

Project Advisor: Associate Professor Santi Pailoplee, Ph.D.

Date of submission/...../.....

Date of approval/...../.....

.....

(Assoc. Prof. Santi Pailoplee, Ph.D.)

Project Advisor

พัชราพร เพ็ชรดี : กลไกการเกิดแผ่นดินไหวตามเขตมุดตัวของเปลือกโลก กลุ่มหมู่เกาะอินโดนีเซีย (FOCAL MECHANISM ALONG THE SUBDUCTION ZONE, INDONESIAN ARCHIPELAGO) อ.ที่ปรึกษาโครงการหลัก: รศ. ดร. สันติ ภัยหลบลี้, 61 หน้า.

การชนกันและการมุดตัวระหว่างแผ่นเปลือกโลกอินโด-ออสเตรเลียกับแผ่นเปลือกโลกยูเรเชีย ส่งผลให้บริเวณกลุ่มหมู่เกาะอินโดนีเซียมีพิบัติภัยแผ่นดินไหวและสึนามิสูง ตามทฤษฎี สึนามิเกิดจากแผ่นดินไหวที่ทำให้เกิดการเปลี่ยนแปลงในแนวตั้งบริเวณพื้นทะเล จุดมุ่งหมายหลักของการศึกษานี้คือ 1) ศึกษาความเสี่ยงในการเกิดสึนามิตามแนวหมู่เกาะอินโดนีเซีย และ 2) ศึกษาความเค้นในแผ่นเปลือกโลกที่มุดตัว ในการศึกษาครั้งนี้ ใช้ข้อมูลจำนวน 2,998 เหตุการณ์ รวบรวมจากฐานข้อมูลกลไกการเกิดแผ่นดินไหวของหน่วยงาน Global CMT ซึ่งข้อมูลกลไกการเกิดแผ่นดินไหวประกอบด้วยข้อมูลการวางตัวของรอยเลื่อนและการเลื่อนตัว จากนั้น ข้อมูลถูกจัดแบ่งออกเป็น 2 ชุดตามสภาพแวดล้อมธรณีแปรสัณฐาน (seismotectonic setting) ได้แก่ แผ่นดินไหวที่เกิดระหว่างขอบของการชนกันของแผ่นเปลือกโลก (ความลึก 0-50 กม.) และแผ่นดินไหวที่เกิดบริเวณแผ่นที่มุดลงไปใต้น้ำในชั้นเนื้อโลก (ความลึกมากกว่า 50 กม.) ในกรณีของแผ่นดินไหวที่เกิดระหว่างขอบของการชนกันของแผ่นเปลือกโลก ผลการศึกษาชี้ว่าบริเวณเนินหน้าร่องลึกก้นสมุทรวา-ซุมบา และแอ่งอารูมีความสามารถในการก่อให้เกิดสึนามิสูงกว่าบริเวณอื่น (คลื่นสึนามิแรกเริ่มสูง 0.65-0.73 เมตร จากแผ่นดินไหวขนาด 7.6) นอกจากนี้ ยังพบเขตรอยเลื่อนใหม่ในบริเวณทะเลบันดาใต้ จากความตรงกันของข้อมูลกลไกการเกิดแผ่นดินไหวและแนวของจุดศูนย์กลางแผ่นดินไหว สามารถวิเคราะห์ได้ว่าเขตรอยเลื่อนนี้วางตัวในแนวตะวันออกเฉียงเหนือ-ตะวันตกเฉียงใต้ และมีการเลื่อนตัวในแนวระดับแบบซ้ายเข้า สำหรับแผ่นดินไหวที่เกิดระหว่างขอบของการชนกันของแผ่นเปลือกโลก ผลการศึกษาชี้ว่าแผ่นเปลือกโลกถูกบีบอัดในความลึกระหว่าง 300-700 กม. ในขณะที่ในความลึกปานกลาง (50-300 กม.) แผ่นเปลือกโลกได้มีความเค้นที่แตกต่างกันในแต่ละบริเวณ ซึ่งเป็นผลมาจากองค์ประกอบของแผ่นเปลือกโลกที่แตกต่างกันรวมไปถึงแรงเค้นจากแหล่งอื่นๆ ดังนั้น นอกจากพิบัติภัยแผ่นดินไหวแล้ว ควรจะศึกษาการบรรเทาพิบัติภัยสึนามิบริเวณเนินหน้าร่องลึกก้นสมุทรวา-ซุมบาและแอ่งอารู รวมไปถึงศึกษาเขตรอยเลื่อนที่พบใหม่ในบริเวณทะเลบันดาใต้

ภาควิชา	ธรณีวิทยา	ลายมือชื่อนิสิต.....
สาขาวิชา	ธรณีวิทยา	ลายมือชื่ออ.ที่ปรึกษาหลัก.....
ปีการศึกษา	2560	

5732740023 : MAJOR GEOLOGY

KEYWORDS: FOCAL MECHANISM / SEISMICITY / INDONESIAN ARCHIPELAGO

PATCHARAPORN PETCHDEE: FOCAL MECHANISM ALONG THE SUBDUCTION ZONE, INDONESIAN ARCHIPELAGO. ADVISOR: ASSOC. PROF. SANTI PAILOPLEE, Ph.D., 61 pp.

From the collision and subduction between Indo-Australian and Eurasian tectonic plates, the Indonesian Archipelago is exposed to high earthquake and tsunami hazards. Theoretically, tsunamis are formed when an earthquake causes vertical displacement at the seafloor. The main aims of this study are i) to evaluate tsunami risks along the Indonesian Archipelago and ii) to determine the stress states in the subducting slabs. In this study, a total of 2,998 focal mechanism solutions were obtained from the Global CMT project. The data contain information of fault plane orientation and fault movement. Seismotectonically, the data were divided into 2 settings, interplate earthquakes (focal depth between 0-50 km) and intraslab earthquakes (focal depth more than 50 km). The result suggested that, in case of interplate earthquakes, Java-Sumba Outer-rise segment and Aru Trough segment, both of which are defined as normal faulting regions, are able to generate relatively high initial tsunamis (0.65-0.73 m from a Mw 7.6 earthquake). In addition, a new seismogenic fault zone has been found in the South Banda Sea. From the consistency of the focal mechanism solutions and the trend of the earthquakes, this fault zone is NE-SW left-lateral strike-slip fault. In case of intraslab earthquakes, the result showed that the slabs are experiencing down-dip compression between the depths of 300-700 km, while at intermediate depths (50-300 km) the stress states are variable in different slabs due to heterogeneous slab compositions and other stress sources. Hence, apart from earthquake, a tsunami mitigation should be conducted along Java-Sumba Outer-rise and Aru Trough. Also, more research is needed to study the newly found fault zone in the South Banda Sea.

Department: Geology

Student's Signature.....

Field of Study: Geology

Advisor's Signature.....

Academic Year: 2017

ACKNOWLEDGEMENTS

This report would not have been achieved without help, suggestion and support from many people. Firstly, I would like to express my sincere appreciation to my advisor, Associate Professor Dr. Sati Pailoplee, whom always gave me advice, guidance, and encouragement since the beginning of this study to the very end of my undergraduate student life. I would like extend my grateful thanks to all professors at Department of Geology, Faculty of Science, Chulalongkorn University for giving me fundamental geological knowledge as well as looking after me for these 4 years in the department.

I also deeply thank all staff members at Seismological Bureau, Thai Meteorological Department especially Mr. Santawat Sukrungsri for providing technical knowledge as well as helping me out with the programming.

My special thanks are also extended to my GEO'58 friends, especially Mr. Natcharphol Charnsiri, Ms. Boontigan Kuhasubpasin, Ms. Narudee Saikrasin, and Ms. Pitchayawee Kittitananuvong for their help, friendship, and consolation when I was depressed.

Finally, I wish to thank my parents for their support and encouragement throughout my study.

CONTENTS

	Page
ABSTRACT	iv
ACKNOWLEDGEMENTS	vi
CONTENTS	vii
LIST OF TABLES	ix
LIST OF FIGURES	x
CHAPTER 1 INTRODUCTION	
1.1. Background	1
1.2. Objective	2
1.3. Study Area	2
1.4. Scope of the Study	2
1.5. Expected Outcomes	2
CHAPTER 2 THEORY AND METHODOLOGY	
2.1. Regional Tectonic Setting	3
2.2. Theory of Focal Mechanism	5
2.2.1. P-wave first motion	6
2.2.2. Beach ball diagram	7
2.2.3. Fault plane solution data	9
2.3. Previous Works	11
2.4. Methodology	15
CHAPTER 3 DATA AND STATISTIC	
3.1. Data	18
3.2. Seismotectonic Setting	22
3.2.1. Terminology	22
3.2.2. Seismotectonic setting of the Indonesian Archipelago	23
3.3. Fault Plane Determination	25
3.3.1. Fault Plane Determination of Interplate Earthquakes	25
3.3.1. Fault Plane Determination of Intraslab Earthquakes	27

	Page
CHAPTER 4 FOCAL MECHANISMS ALONG THE INDONESIAN ARCHIPELAGO	
4.1. Focal Mechanism of the Study Area	30
4.2. Focal Mechanism of Interplate Earthquakes	31
4.3. Focal Mechanism of intraslab Earthquakes	37
CHAPTER 5 DISCUSSION AND CONCLUSION	
5.1. Interplate Earthquakes	41
5.1.1. Focal mechanism solutions of interplate earthquakes	41
5.1.2. Tsunami generation along the Indonesian Archipelago	46
5.2. Intraslab Earthquakes	49
5.2.1. Focal mechanism solutions of intraslab earthquakes	49
5.2.2. Seismotectonic models of subducting slabs	50
5.3. Conclusion	55
5.4. Recommendation	56
REFERENCES	57

LIST OF TABLES

		Page
Table 3.1.	FMS of the largest earthquakes ($M_w > 7.0$) in the study area.	21
Table 3.2.	Contour maps and rose diagrams showing the distribution of each FMS parameter of interplate earthquakes' nodal plane 1.	26
Table 3.3.	Contour maps and rose diagrams showing the distribution of each FMS parameter of interplate earthquakes' nodal plane 2.	27
Table 3.4.	Contour maps and rose diagrams showing the distribution of each FMS parameter of intraplate earthquakes' nodal plane 1.	28
Table 3.5.	Contour maps and rose diagrams showing the distribution of each FMS parameter of intraplate earthquakes' nodal plane 2.	29
Table 4.1.	Rake-based ternary plots, contour P-T maps, and FMS of each interplate sub-region. Noted: Blue = P-axis, Red = T-axis.	33
Table 4.2.	Rake-based ternary plots, contour P-T maps, and FMS of each intraslab sub-region. Noted: Blue = P-axis, Red = T-axis.	39
Table 5.1.	Preferred fault plane orientation and slip rake of interplate earthquakes.	41
Table 5.2.	Average vertical seafloor displacement of each interplate sub-region. Note: Negative VS indicates hanging wall moving down, Positive VS indicates hanging wall moving up.	48
Table 5.3.	P- and T-axis orientation of each average FMS of intraslab earthquakes.	50

LIST OF FIGURES

		Page
Figure 1.1.	Map of the Indonesian Archipelago showing the subduction between Indo- Australian plate and Eurasia plate (Pailoplee, 2017).	2
Figure 2.1.	Tectonic setting of the South East Asia Region. The vectors represent relative velocity between plates as labeled. (McCaffrey, 2009).	3
Figure 2.2.	Map of Southeast Asia showing different crust types in the region (Doust and Lijmbach, 1997).	4
Figure 2.3.	Cross section through Java showing the Benioff zone (Hamilton, 1979).	5
Figure 2.4.	P- and S-wave radiation patterns for a earthquake (Barth et al., 2008).	6
Figure 2.5.	First motion of P-waves recorded at seismic station (Grotzinger and Jordan, 2007).	7
Figure 2.6.	Lower hemisphere projection of the seismic station. (A) Ray paths of the seismic wave radiating from an earthquake to seismic stations. (B) Location of the seismic station plotted on the stereonet at the azimuth of 50° and take-off angle of 60° (Stein and Wysession, 2003).	8
Figure 2.7.	Fitting planes to data from a hypothetical earthquake (Norton, 2008).	8
Figure 2.8.	Beach ball diagrams for different fault geometries. Compression quadrants are dark, dilatation quadrants are white. The thrust and normal mechanisms are for 45° dipping, N-S trending pure dip-slip fault. The pure strike-slip fault mechanism is for vertical, NE-SW or NW-SE striking fault (Earthquake Research Committee, 2011).	9
Figure 2.9.	Model showing the strike, dip, and rake of a shear fault. u is a slip vector of the hanging wall (Dai, 2015).	10

	Page
Figure 2.10. Beachball diagrams showing focal mechanisms with the same N-S striking fault planes, but various rakes (λ) (Stein and Wysession, 2003).	11
Figure 2.11. (A) Map showing sub-domains along the Sunda margin. The segmentation was based on the prevailing seismicity. (B) Distribution of anomalous relief, seismicity patterns, the thickness of sediment in the trench, and the age of subducting oceanic plate (Shulgin, 2012).	12
Figure 2.12. POE of an earthquake of Mw within 50 years (Pailoplee, 2017).	13
Figure 2.13. The map showing spatial distribution of z-values along the Indonesian Islands. The prospective areas for moderate-large earthquakes are circled and labeled (Janephanut, 2015).	13
Figure 2.14. Maps showing rake along the SASZ. (A) Interplate earthquakes, (B) Intraslab earthquake (Ketthong, 2016).	14
Figure 2.15. Map showing the FMS and rake of each fault zone in the TLMB (Vajchakorn, 2016).	15
Figure 2.16. Work flow chart	17
Figure 3.1. The GCMT catalogue search (http://www.globalcmt.org/CMTsearch.html).	19
Figure 3.2. Example of the focal mechanism data in GCMT catalogue. The information inside red rectangles are the ones used in this study.	20
Figure 3.3. Map showing the distribution of all 2,998 FMS data used in this study.	20
Figure 3.4. Model showing different types of earthquakes in the subduction zone based on their seismotectonic setting. A= interplate earthquakes, B=intraplate earthquakes, C=intraslab earthquakes (Pailoplee, 2018).	22
Figure 3.5. Map showing the distribution of the earthquakes in the Indonesian Archipelago. Section 3 and Section 4 are cross-sections showing the distribution of earthquake (grey dots) in the SSZ (Charusiri and Pailoplee, 2015).	

	Page	
Figure 3.6.	Histogram showing distribution of focal depth of earthquakes used in this study. Green line indicates the depth of 50 km which is the cutoff depth separating interplate and intraslab earthquakes.	24
Figure 3.7.	Map showing the location and the FMS of the interplate earthquakes.	24
Figure 3.8.	Map showing the location and the FMS of the intraslab earthquakes.	24
Figure 4.1.	Ternary diagram showing the distribution of faulting mechanisms of all events. The classification is based on Frohlich and Anderson (1992).	30
Figure 4.2.	Contour map of (A) P-axes (B) T-axes of all events.	31
Figure 4.3.	Ternary diagram showing the distribution of faulting mechanisms of interplate earthquakes. The classification is based on Frohlich and Anderson (1992).	31
Figure 4.4.	Contoured map of (A) P-axes (B) T-axes of interplate earthquakes.	32
Figure 4.5.	Map showing sub-regions of Interplate earthquakes.	37
Figure 4.6.	Ternary diagram showing the distribution of faulting mechanisms of intraslab earthquakes. The classification is based on Frohlich and Anderson (1992).	37
Figure 4.7.	Contour map of (A) P-axes (B) T-axes of intraslab earthquakes.	38
Figure 4.8.	Map showing sub-regions of Intraslab earthquakes.	38
Figure 5.1.	Map showing an average focal mechanism of each interplate sub-region. Thick black lines are preferred fault planes. Faulting mechanisms are represented in different colours, red = normal faulting, blue = reversed faulting, green = strike-slip faulting.	42
Figure 5.2.	Map showing interpret fault zones. Each colour represents each fault zone; purple = the SSZ, pink = the Sumatran Fault Zone, orange = Java-Sumba Outer-rise, Cyan = Flores and Wetar Thrusts, green = South Banda Sea, yellow = Sorong Fault Zone, emerald green = West Papua Subduction, blue = Tarera-Aiduna Fault Zone, red = Aru Trough.	42

	Page
Figure 5.3. Structure and Kinematics of the Great Sumatran Fault Zone. (A) Real-scale 3D view of the tectonic configuration of the northern sector of the Sumatran section of the Sunda arc. (B) Idealized block diagram showing the geometry of the Sliver plate and overall motions under oblique subduction (Fernández-Blanco et al., 2016).	44
Figure 5.4. Generalized diagram of a subduction zone showing types of fault ruptures (modified from Geist, 1998).	44
Figure 5.5. Digital elevation model of the Banda Arc region showing active faults (Standley and Harris, 2009).	45
Figure 5.6. Maps showing (A) detailed seafloor bathymetry of Aru Trough, and (B) normal faults that border Aru and Tanimbat Through (Hall et al., 2017).	45
Figure 5.7. Map showing the lineament (red dashed line) that may be responsible for left-lateral strike-slip earthquakes in the South Banda Sea. Orange dots are earthquakes occurring in the region (modified from Standley and Harris, 2009).	46
Figure 5.8. Fault geometry model. Note: ϕ = strike, δ = dip angle, and λ = slip rake (modified from Maher, 2017).	48
Figure 5.9. Initial height of tsunami along the Indonesian Archipelago.	49
Figure 5.10. Map showing an average focal mechanism of each intraplate sub-region. Faulting mechanisms are represented in different colors, red = normal faulting, blue = reversed faulting.	50
Figure 5.11. Earthquakes observed at subduction zones (Stein and Wysession, 2003).	51
Figure 5.12. Examples of cross sections of seismicity across different subduction zones (Isacks and Molnar, 1971).	51
Figure 5.13. Map showing the location of (A) Sumatra slab (B) Java slab (C) Flores slab (D) Banda Arc slab.	52
Figure 5.14. 3D seismotectonic model of the Sumatra slab.	52
Figure 5.15. 3D seismotectonic model of the Java slab.	53

	Page
Figure 5.16. 3D seismotectonic model of the Flores slab.	54
Figure 5.17. Map showing the transitional zone between Indian oceanic plate and Australian continental plate (modified from Stagg, 1978).	54
Figure 5.18. 3D seismotectonic model of the Banda Arc slab.	55

CHAPTER 1

INTRODUCTION

1.1. Background

The Indonesian Archipelago extends from Sumatra Island in the west to Aru Island in the east, then curves 180° to the north towards North Banda Sea (Spakman and Hall, 2010). Tectonically, the Indonesian Archipelago is a result of the north-south plate collision and subduction of Indo- Australian plate beneath Eurasia plate (Krabbenhoeft et al., 2010). Based mainly on the GPS data, the subduction velocity ranges from 50 to 70 mm/yr (Simmons et al., 2007). The Indonesian Archipelago is regarded as a seismic active region although the seismic activities in this area is relatively low comparing to those of the Sumatra-Andaman subduction zone. However, the record shows that most of the earthquakes occurred in the Indonesian Archipelago caused tsunami (Ammon et al., 2006). The most recent tsunami-generated earthquake in the region is the Mw-7.8 Mentawai earthquake on October 25, 2010 with at least 445 people killed (Hill et al., 2012). According to the National Oceanic and Atmospheric Administration (NOAA), there are more than 150 major earthquakes within past 380 years (1629-2010) which generated tsunami that struck the Indonesia Islands.

Focal mechanism or fault plane solution is a result of analysis of seismic wave forms generated by an earthquake (Shah, 2015). It shows the alignment of the fault plane and the slip direction of the fault, which let us understand the mechanism of the earthquake faulting. However, determining the focal mechanism takes quite a long time, few hours for rapid determination and 3-4 months for systematic determination. (Elström et al., 2012)

To understand the trends of the earthquake mechanisms as well as the tsunami probabilities along the Indonesian Archipelago, this study focus on evaluating the patterns of the focal mechanism and determining the stress regimes in the region using a statistic approach based upon the Global CMT catalogue reporting systematically focal mechanism data. The obtained results should be useful to improve the estimation of the tsunami hazard level, i. e. , vertical displacement during the earthquake, which will help decreasing the fatalities and damage from tsunami that hit the communities located along the Indonesian Archipelago and neighboring regions.

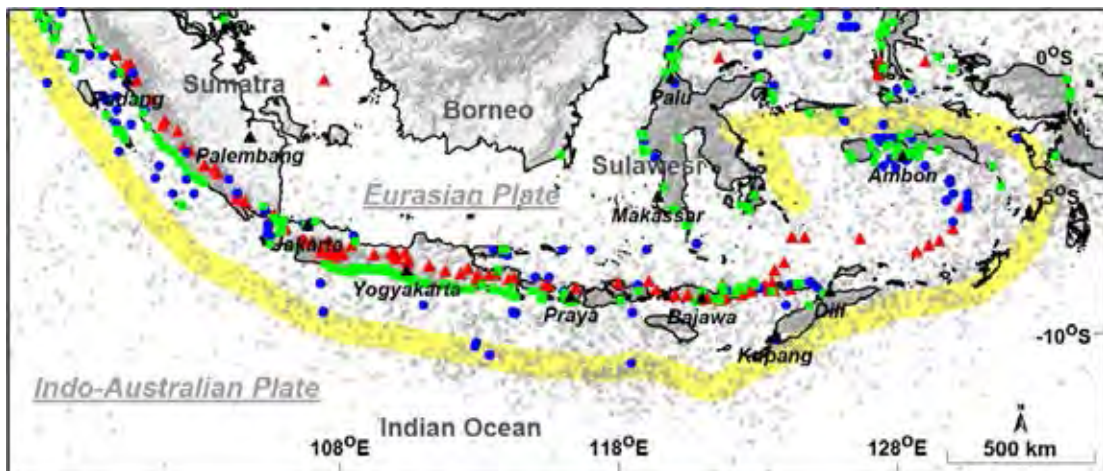


Figure 1.1. Map of the Indonesian Archipelago showing the subduction between Indo-Australian plate and Eurasia plate (yellow line). Red triangles represent active volcanoes. Blue dots are the tsunami earthquake epicenters and the green squares are tsunami run-ups. Grey dots show the location of all earthquake epicenters (Pailoplee, 2017).

1.2. Objective

To evaluate the patterns of the mechanism of faulting along the Indonesian Archipelago, using focal mechanism data.

1.3. Study Area

The study area is the Indonesian Archipelago as shown in Figure 1.1. It covers the area between latitude interval of 15.1°S-1.51°N and longitude interval of 96.08-135.47°E.

1.4. Scope of the Study

Investigating the trend of the faulting and rupturing of the earthquake sources using focal mechanism data recorded within the study area. The focal mechanism data used in the study are obtained from the Global CMT catalogue.

1.5. Expected Outcomes

- 1.5.1 The pattern of earthquake mechanism along the Indonesian Archipelago
- 1.5.2 Primary model of the geometry and movement of subducting slab in the Indonesian Archipelago

CHAPTER 2

THEORY AND METHODOLOGY

2.1. Regional Tectonic Setting

The Indonesian Archipelago lies on the southern border of the Sunda plate. The Australian plate subducting beneath the Sunda plate results in the formation of the Indonesian Archipelago and Sunda trench, high seismicity, and volcanic activities in the area. According to Hamilton (1974, 1979), this subduction zone is part of larger convergent belt which extends from the Himalayas to Myanmar to the Indonesian Archipelago and bends to the north around Banda sea (Figure 2.1). The subduction south of Java, Sunda Islands (Sumba, Timor), and east of Banda arch is known as the Sunda Subduction Zone (SSZ), while the subduction to the north (west of Andaman Islands and Sumatra) is called the Sumatra-Andaman Subduction Zone.

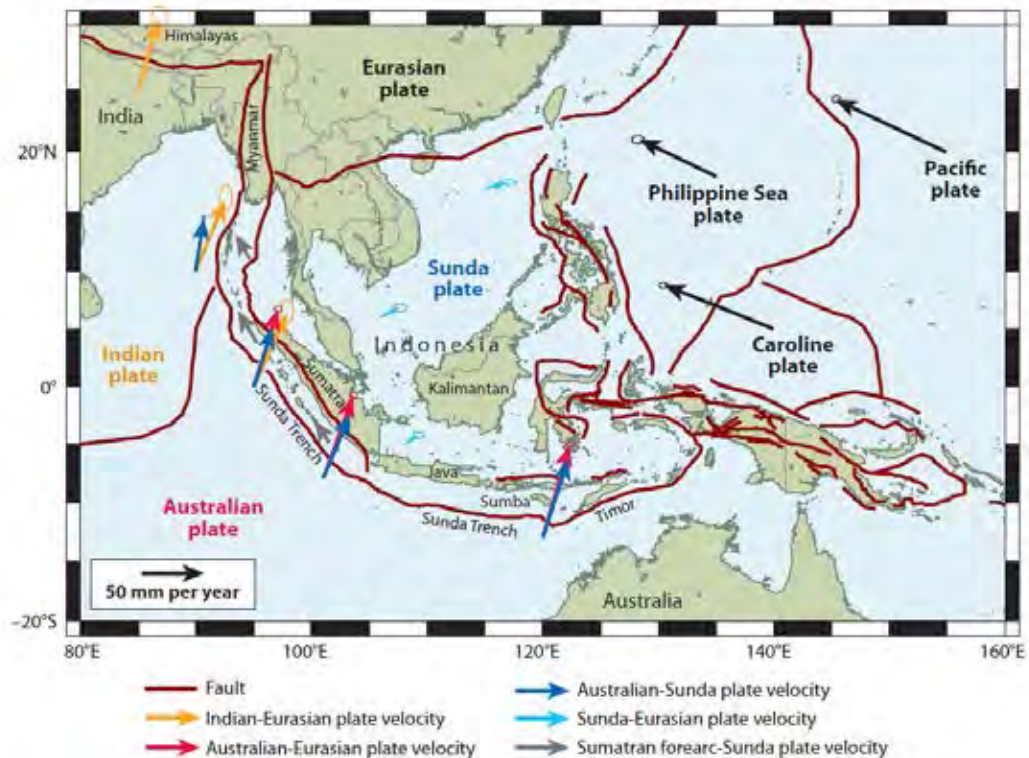


Figure 2.1. Tectonic setting of the South East Asia Region. The vectors represent relative velocity between plates as labeled (McCaffrey, 2009).

The NNE motion of the Indo-Australian plate causes the oblique subduction in the SSZ. However, the subduction is almost normal off Java and further to the East. Based mainly on the GPS data, the convergence rate increases southeastwards, ranging from 40-50 mm/year off Sumatra to 70 mm/year off Java and Bali (Simmons et al., 2007). The dense lithosphere of the Indian Oceanic plate subducts beneath the continental Sunda shelf in the west of Sumba (McCaffrey, 2009). To the east, Banda arc's iconic shape results from subduction of the continental Australian lithosphere under oceanic crust (Spakman and Hall, 2010). The dips of Wadati-Benioff zone of mantle earthquakes in the SSZ steepen downwards the subducting slab (Hamilton, 1979).

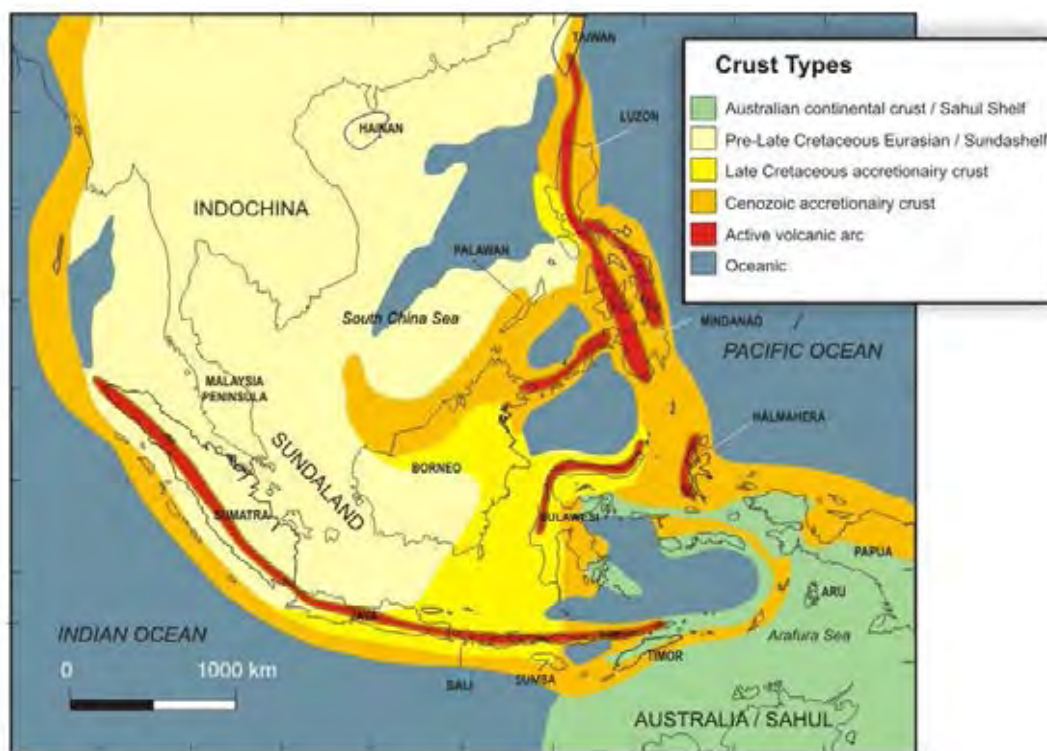


Figure 2.2 Map of Southeast Asia showing different crust types in the region (Doust and Lijmbach, 1997).

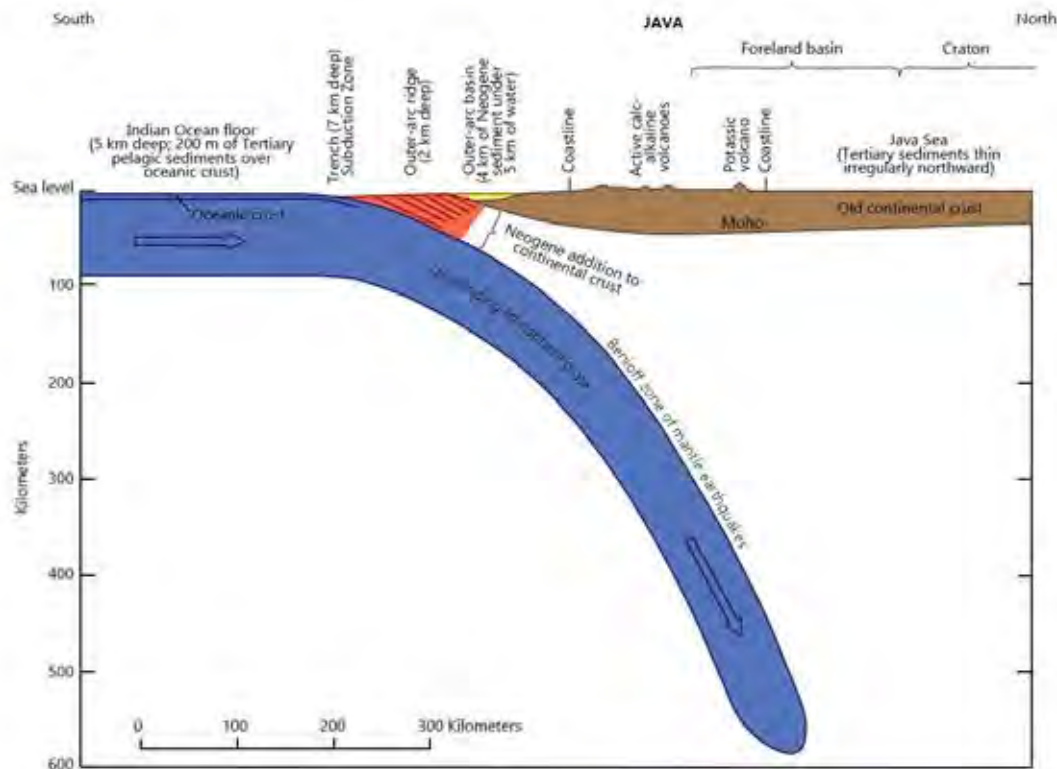


Figure 2.3. Cross section through Java showing the Benioff zone (Hamilton, 1979).

2.2. Theory of Focal Mechanism

Focal mechanism is a method used to study the faulting mechanism of the earthquake. A focal mechanism solution (FMS) or fault plane solution is a result of an analysis of seismic waves generated from an earthquake. The patterns of these waves radiating from the focus mainly depend on the fault's geometry and the slip motion (Stein and Wysession, 2003). To generate an acceptable FMS, it takes at least 10 records of waveforms and the location of the seismograph stations used must be well distributed around the epicenter. The complete FMS contains the information of origin time, location of the epicenter, focal depth, scalar moment, magnitude and components of the moment tensor. The orientation of the fault plane and the sense of slip can be determined by using the moment tensor (Cronin, 2010).

To determine the FMS, several methods are used such as P-waves first motion, polarization and amplitude of S-wave (e.g. Khattri, 1973), the analysis of P/S amplitude ratios (e.g. Kisslinger et al., 1981) and moment tensor inversion (e.g. Stein and Wysession, 2003). The P-waves first motion and moment tensor inversion are the most

used ones. These methods use the radiation pattern of seismic waves that convey the orientation of the fault and the slip occurs during the earthquake.

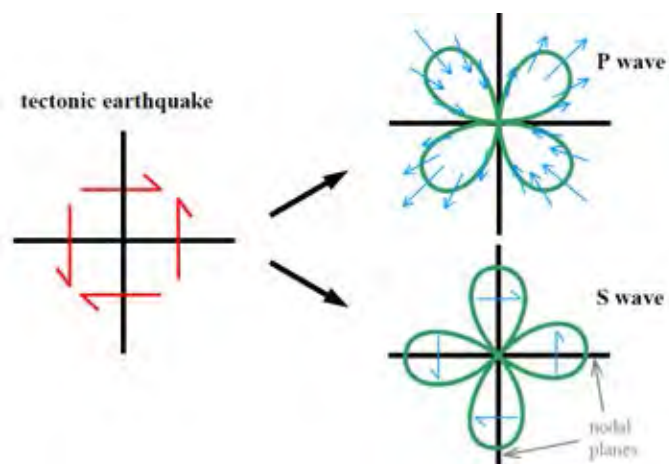


Figure 2.4. P- and S-wave radiation patterns for a earthquake (Barth et al., 2008).

2.2.1. P-wave first motion

The basic idea of this method is the arrival of P-wave at each station in different direction varies due to the movement of fault relative to the station. The first vertical motion of P-wave of is up (or compressional) if the materials near fault moving toward the station, or down (dilatational) if the materials moving away from the station (Figure 2.5). The first motions define 4 quadrants, 2 compressional and 2 dilatational separated by a fault plane and a plane perpendicular to it (auxiliary plane). These two planes are also called 'nodal planes' because P-waves radiate parallel to these plane show zero first motion (Stein and Wysession, 2003). However, the first motions from the slips on these two planes are identical. To identify the actual fault plane needs additional information, such as a known fault trend, ground motion, or the trend of aftershocks.

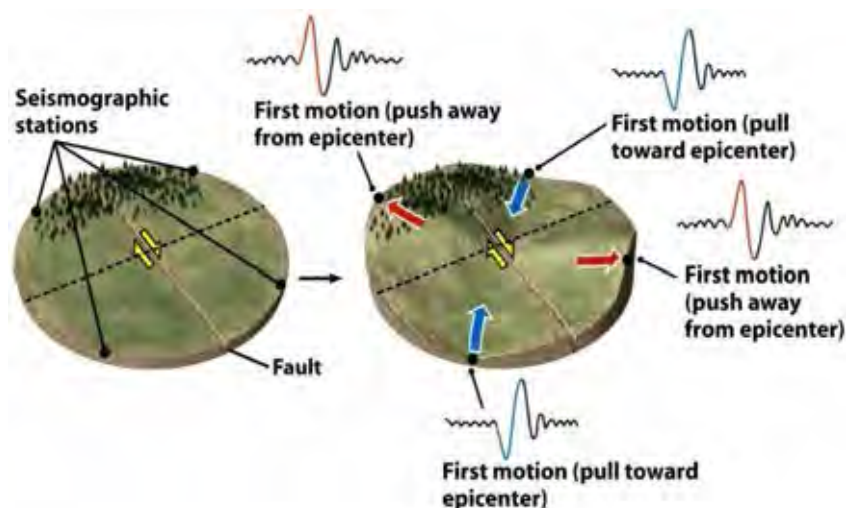


Figure 2.5. First motion of P-waves recorded at seismic station (Grotzinger and Jordan, 2007).

2.2.2. Beach ball diagram

The FMS are usually presented in lower-hemisphere stereographic projections, known as beach ball diagrams. To generate the FMS as well as beach ball diagram, locations of the seismograph station are projected on the focal sphere corresponding with emerging ray at each station. Each station is marked according to the first motion, compressional or dilatational, and plotted regarding to the azimuth and angular distance (take-off angle) relative to the focus of the earthquake, which is represented as the center of the stereonet (Figure 2.6). Then two orthogonal planes are defined to separate the compressional points from dilatational points (Figure 2.7). The P- and T- axes defined as the center of the compressed and dilatated quadrants respectively. The point where 2 nodal planes intersect is N-axis (or B-axis).

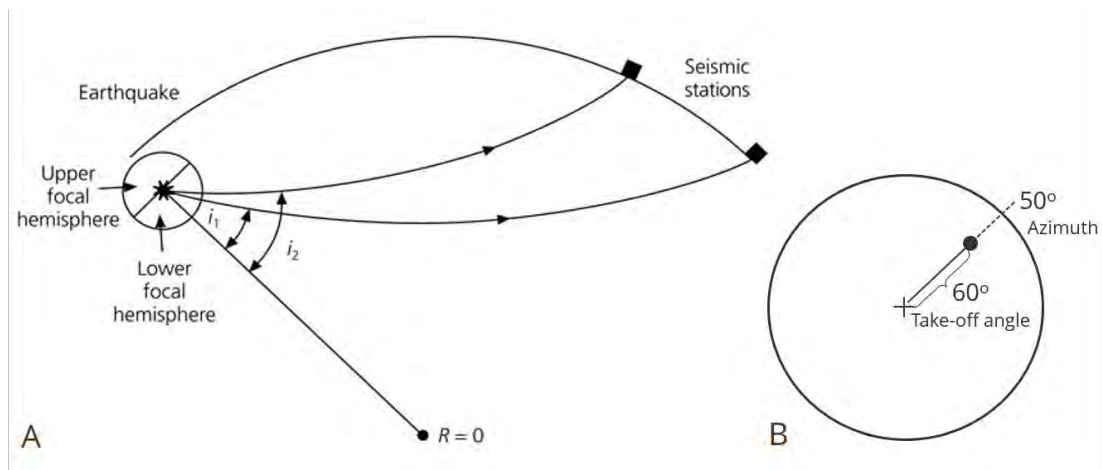


Figure 2.6. Lower hemisphere projection of the seismic station. (A) Ray paths of the seismic wave radiating from an earthquake to seismic stations. Take-off angle or angle of incidence (i) is an angle between imaginary vertical line and ray path as it just emerges from the source, as well as the angle the ray intersects the lower focal hemisphere. (B) Location of the seismic station plotted on the stereonet at the azimuth of 50° and take-off angle of 60° (Stein and Wysession, 2003).

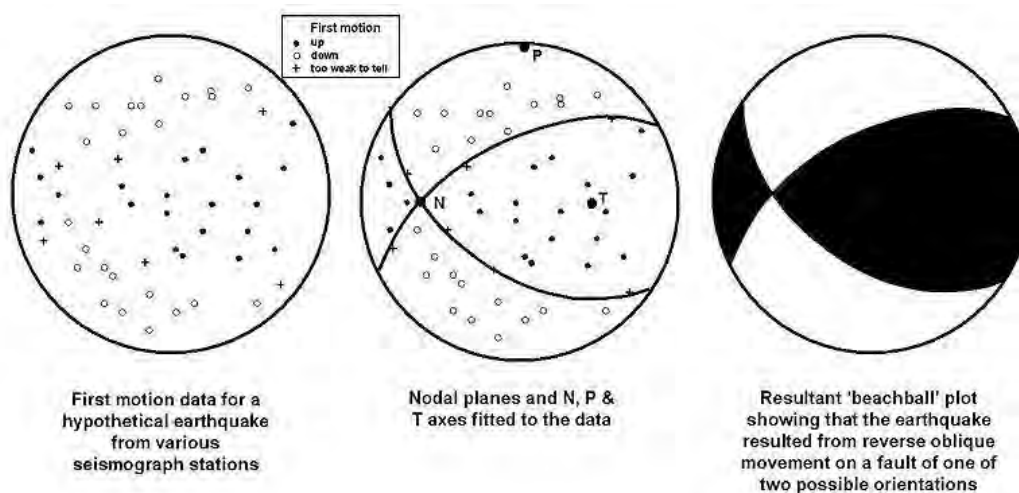


Figure 2.7. Fitting planes to data from a hypothetical earthquake (Norton, 2008).

Different types of faulting appear differently on beach ball diagram. The black/ dark and white quadrants, representing the compression and dilatation respectively, show the geometry of the fault (Figure 2.8). Even though the beach ball diagrams look different, they all represent the same P- wave radiation pattern. However, because of the orientation of the fault planes and senses of slip are vary

relative to the Earth's surface, the projections of radiation lobes on lower hemisphere diverge (Norton, 2008).

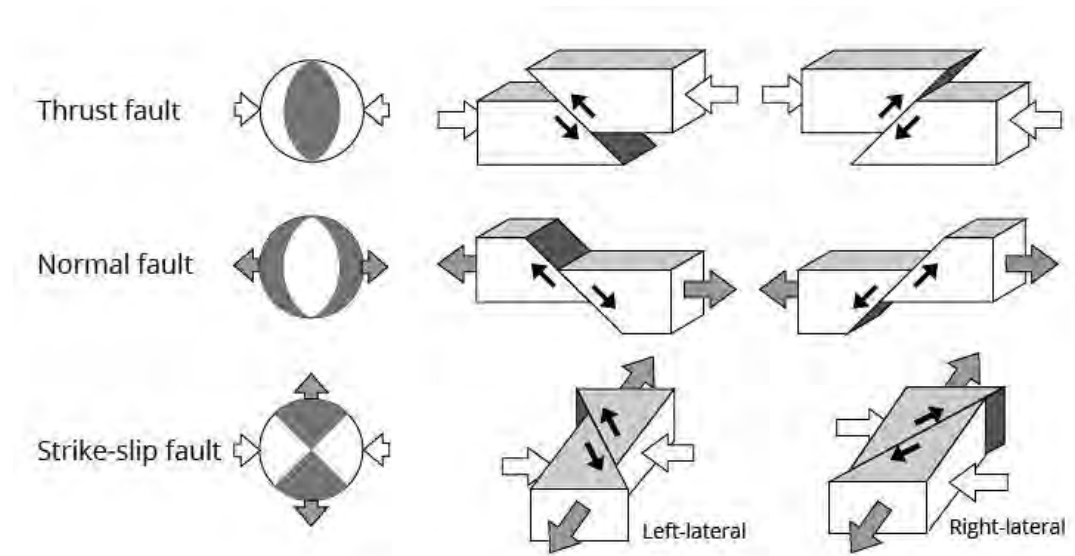


Figure 2.8. Beach ball diagrams for different fault geometries. Compression quadrants are dark, dilatation quadrants are white. The thrust and normal mechanisms are for 45° dipping, N-S trending pure dip-slip fault. The pure strike-slip fault mechanism is for vertical, NE-SW or NW-SE striking fault (Earthquake Research Committee, 2011).

2.2.3. Fault plane solution data

The FMS contain 2 sets of plane orientation and slip motion. The orientation showed as reference strike, using right-hand method, and dip angle of the plane. The slip motion presented in form of 'rake (λ)' or 'slip angle', which is the direction of movement of the fault plane relative to the reference strike (Figure 2.9). If an angle is measured anticlockwise from reference strike, the angle is considered as a positive angle. On the other hand, an angle measured clockwise is a negative one. The permissible rake ranges from -180° to $+180^\circ$.

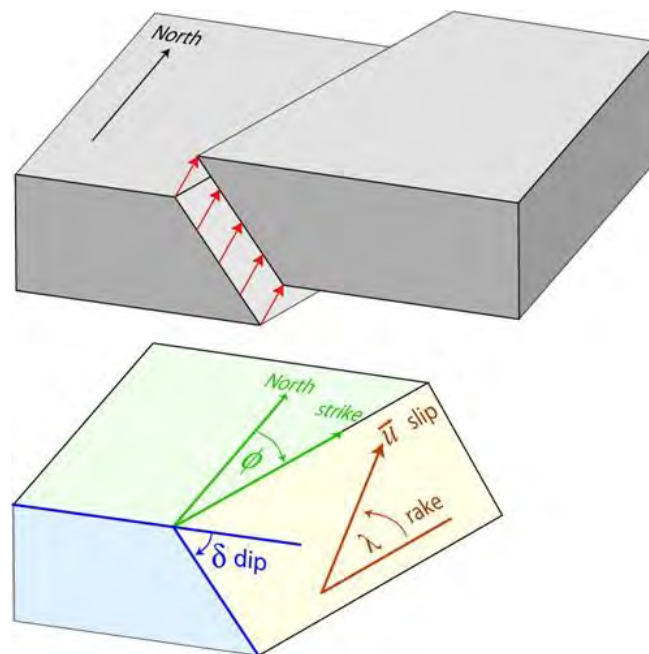


Figure 2.9. Model showing the strike, dip, and rake of a shear fault. u is a slip vector of the hanging wall (Dai, 2015).

The fault geometries can be determined from the values of the rakes. A rake of 90° suggests that the hanging wall moves entirely upwards. Similarly, a rake of -90° indicates a totally downward movement of the hanging wall. A rake of 0° and 180° show strike-slip motions as a left-lateral and right-lateral respectively. Huaksson (1990) grouped earthquakes based on their rake values into normal, reversed, and strike-slip faulting. Normal faults have rakes extending from -45° to -135° while reversed faulting has rakes of 45° to 135° . Strike-slip faults have rakes of ranging from -44° to 44° and -135° to 135° .

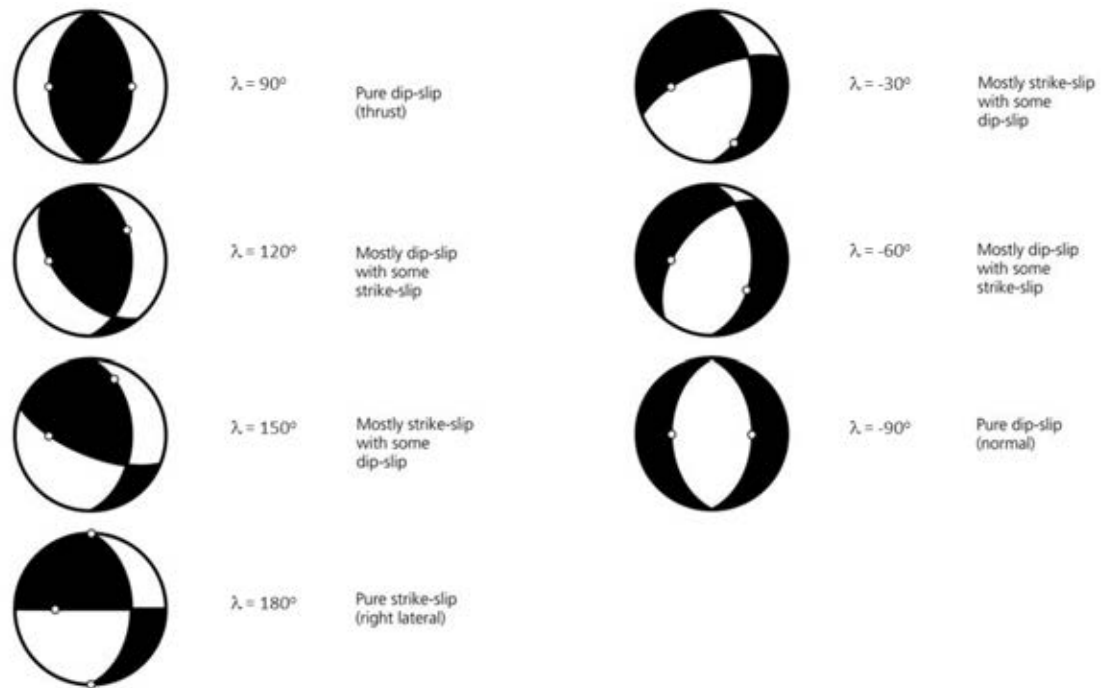


Figure 2.10. Beachball diagrams showing focal mechanisms with the same N-S striking fault planes, but various rakes (λ) (Stein and Wysession, 2003).

2.3. Previous Works

Shulgin (2012) studied segmentation along Sunda Margin, Indonesia, using geophysical and tectonic interpretations. The structural models of the subduction zone were constrained and they show variations of structure of the subduction complex. The study revealed that the thickness of the crystalline crust in the Savu Sea increases as the Australian shelf approaches to the trench, from the normal 7 km thick oceanic crust to 12 km thick crystalline Australian shelf. The theory has been proposed that oceanic subduction is transitioning to continent-arc collision. This interpretation provides explanation of the absence of shallow earthquakes at this segment of the subduction zone. In addition, this study revealed that the thickness of sediment on the oceanic plate is one of the factors controlling the size of the accretionary complexes, which controls the seismogenesis.

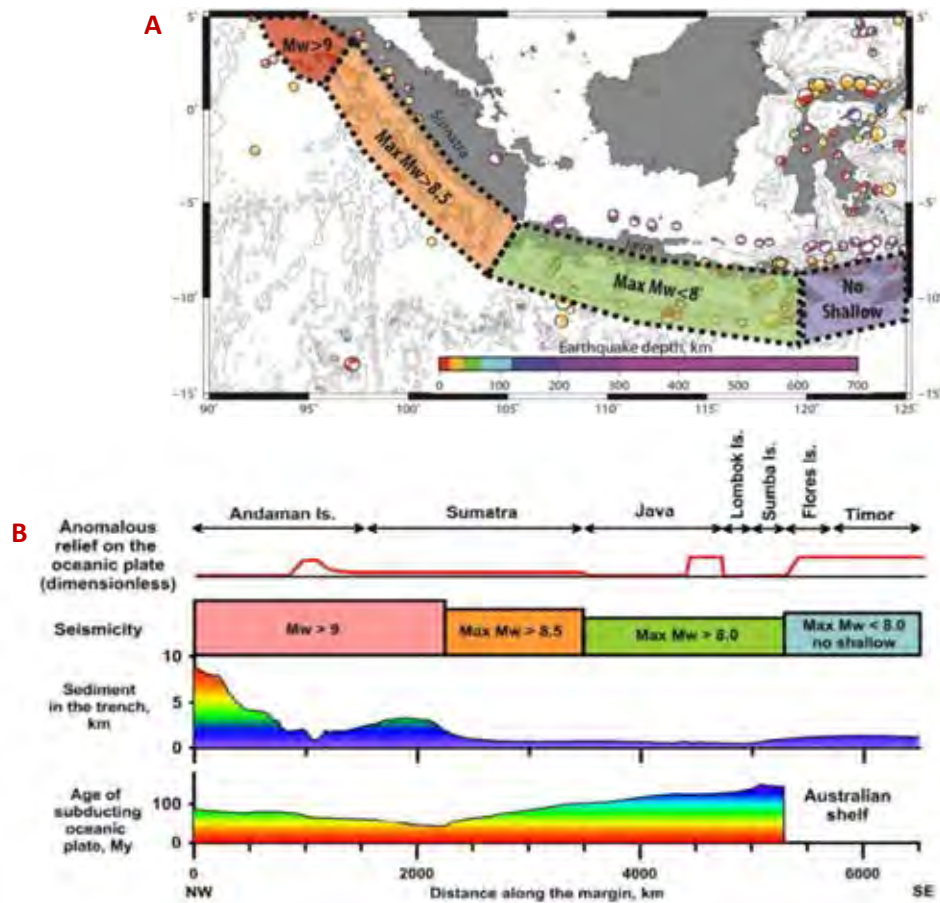


Figure 2.11. (A) Map showing sub-domains along the Sunda margin. The segmentation was based on the prevailing seismicity. (B) Distribution of anomalous relief, seismicity patterns, the thickness of sediment in the trench, and the age of subducting oceanic plate (Shulgin, 2012).

Pailoplee (2017) studied the probability of earthquake activities along the Indonesian Sunda Margin (ISM) using a statistical approach. The a - and b -values obtained from the frequency-magnitude distribution (FMD) relationship have been calculated and mapped. The spatial distributions of the a - and b -values mostly conformed with each other, with higher values in the areas of southern Praya, Kupang, eastern Dili, and eastern Ambon. A comparatively high a -value indicates a high seismicity, while the higher b -value implies the lower ratio of large to small earthquakes. Moreover, the possible maximum magnitude, the return period, and the probability of exceedance (POE) for an earthquake in the ISM were also determined. The results showed that the segment of Jakarta to Padang, surrounding Ambon, and NE Palu was regarded as a high hazardous area, with >50% chance of an earthquake with a maximum M_w up to 8.0

occurring within the next 50 years. Furthermore, the return period of a Mw-7.0 earthquake is 30 years or less.

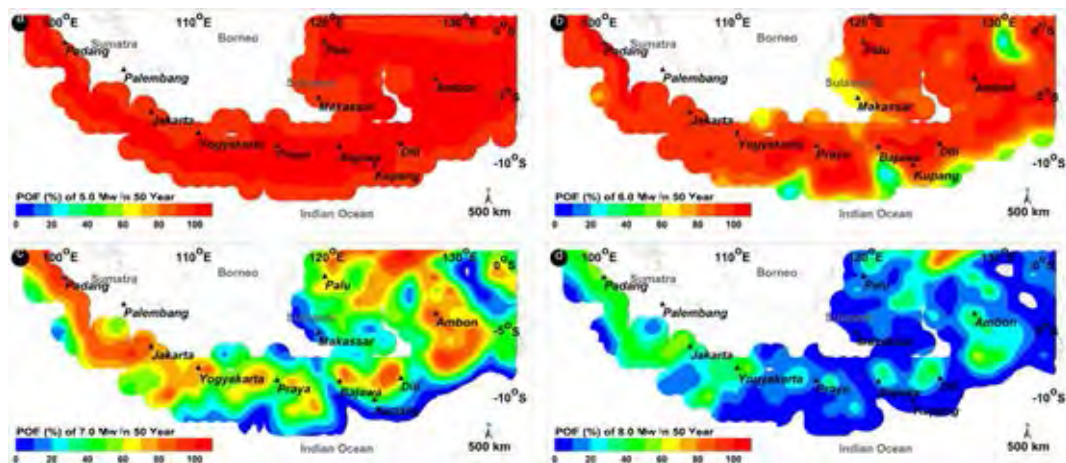


Figure 2.12. POE of an earthquake of Mw within 50 years (Pailoplee, 2017).

Janephanut (2015) studied the spatial distribution of z-values along the Indonesian Islands in order to evaluate prospective areas for upcoming moderate-large earthquakes. Z-value is the change of seismicity rate in the time given. It can be used to detect the seismic quiescence that usually occur before large earthquakes striking. The higher z-values, the lower seismic activities in the area. If the values are really high, it means that the earthquake activities are significantly lower than usual; in another word, there is seismic quiescence in the area. The study shows that there are 3 quiescence-anomaly areas, which are at risk of future moderate-large earthquakes, located at Padang, Jakarta, and Yogyakarta to Praya.

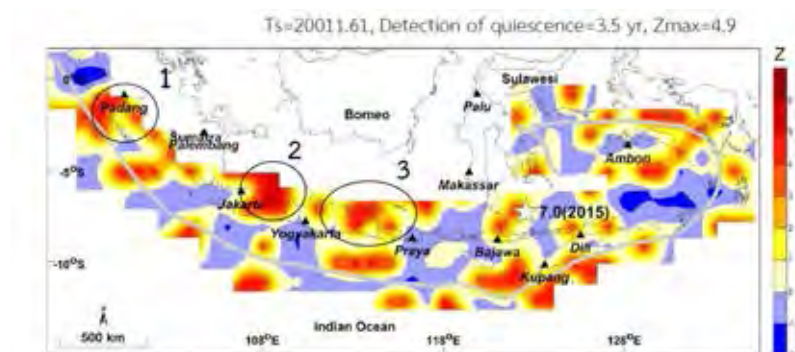


Figure 2.13. The map showing spatial distribution of z-values along the Indonesian Islands. The prospective areas for moderate-large earthquakes are circled and labeled (Janephanut, 2015).

Ketthong (2016) studied the focal mechanism and fractal dimension along the Sumatra-Andaman Subduction Zone (SASZ). The FMS of both interplate and intraslab earthquakes show that both settings are under reverse and oblique faulting regimes with average dip angle of 45° . The SASZ can be divided into 11 segments. For interplate earthquakes, most of the area along the SASZ has vertical motion, which are regarded as tsunami hazardous zones. For intraslab earthquakes, most of the drift faulting motions are vertical. The result of fractal dimension and b-value analysis reveals that the seismic pattern in the SASZ is a plane source.

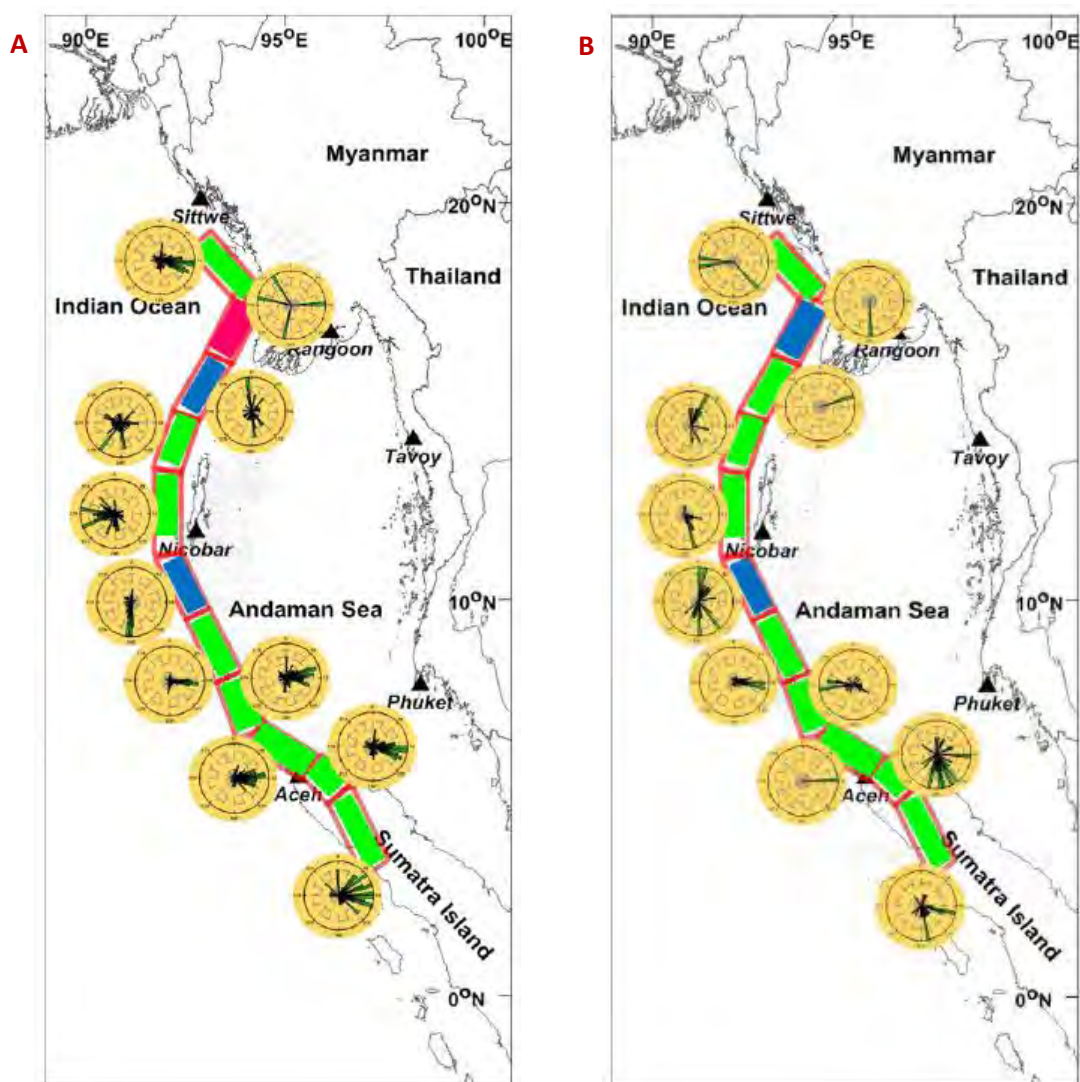


Figure 2.14. Maps showing rake along the SASZ. (A) Interplate earthquakes. (B) Intraslab earthquake. Noted: vertical motion is shown in green, horizontal motion is shown in blue, and distributed motion is shown in pink (Ketthong, 2016).

Vajchakorn (2016) investigated the earthquake mechanisms and patterns of earthquakes occurred in Thailand-Laos-Myanmar border (TLMB), using FMS and fractal dimension analysis. The result shows that the average faults movement in the area is NE-SW striking left-lateral faulting with dip angles varying between 65° – 85° . Moreover, 8 significant fault zones in TLMB were investigated. The FMS shows that all fault zones are left-lateral strike-slip faults except Mae Chan Fault zone which is right-lateral strike-slip fault. Moreover, the result of fractal dimension and b-value analysis reveals that the seismic patterns in almost every area in the TLMB are plane sources.

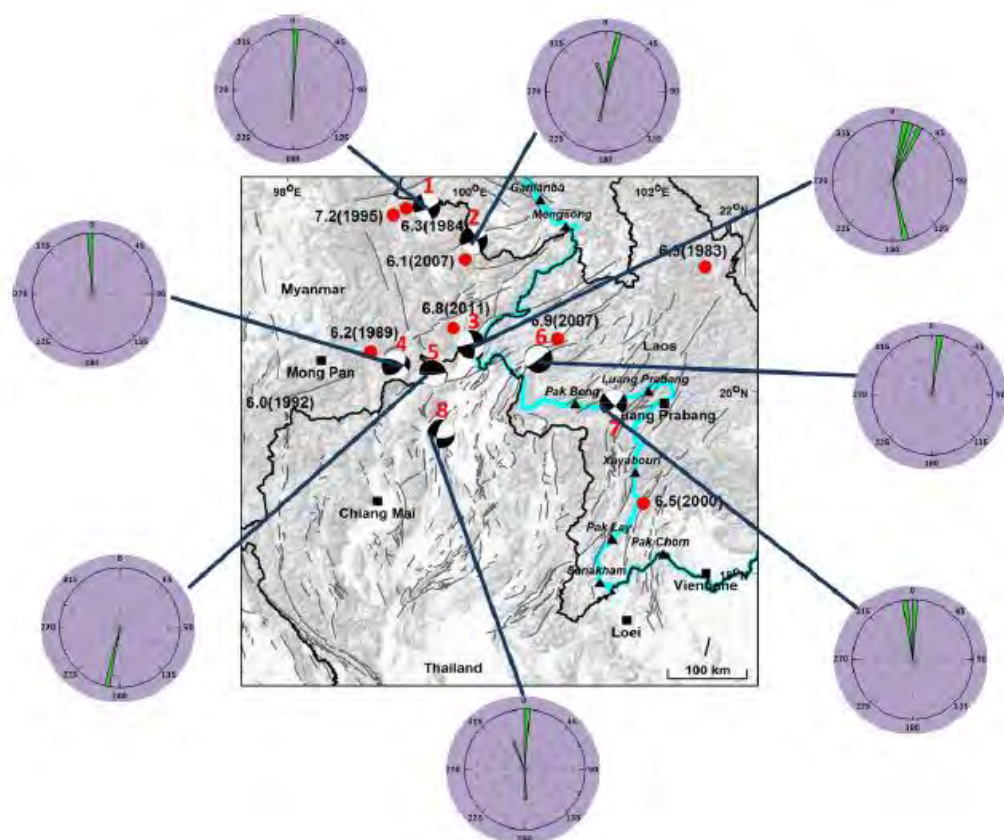


Figure 2.15. Map showing the FMS and rake of each fault zone in the TLMB (Vajchakorn, 2016).

2.4. Methodology

1. Literature review.
2. Acquire the focal mechanism data within the study area from the Global CMT catalogue (www.globalcmt.org). The data contains the information of latitude and

longitude of the earthquake's epicenter, focal depth, fault plane alignment with the slip rake and their conjugates, magnitude, and date and time of the event.

3. Process the data.

a. Plot the histogram of depth distribution of the foci to classify the data based on the seismotectonic setting of the area, interplate earthquakes and intraslab earthquake.

b. Compute contour maps and rose diagrams of both set of strike, dip and rake through Surfer and Grapher programs respectively, in order to determine the actual fault plane of the data set.

c. For each seismotectonic class, sectionize the study area into sub-regions based on the variations in focal mechanism using the contour maps of fault plane's strike, dip angle, and slip rake.

4. Analyze the faulting mechanism characteristic of each sub-region by generating rake based ternary diagrams to evaluate the variation of faulting mechanism, mapping and contouring P- and T-axes to determine the stress regime in the area and computing average focal mechanism (using FaultKin program).

5. Discussion and conclusion.

a. For interplate earthquakes, correlate each sub-region defined in this study to previously defined seismic source zones in the study area. Then, evaluate the initial tsunami height triggered by an earthquake in each sub-region to determine the tsunami hazard potential along the Indonesian Archipelago.

b. For intraslab earthquakes, project the focal mechanism on to the slabs in order to study the stress states within the slabs.

6. Report and presentation

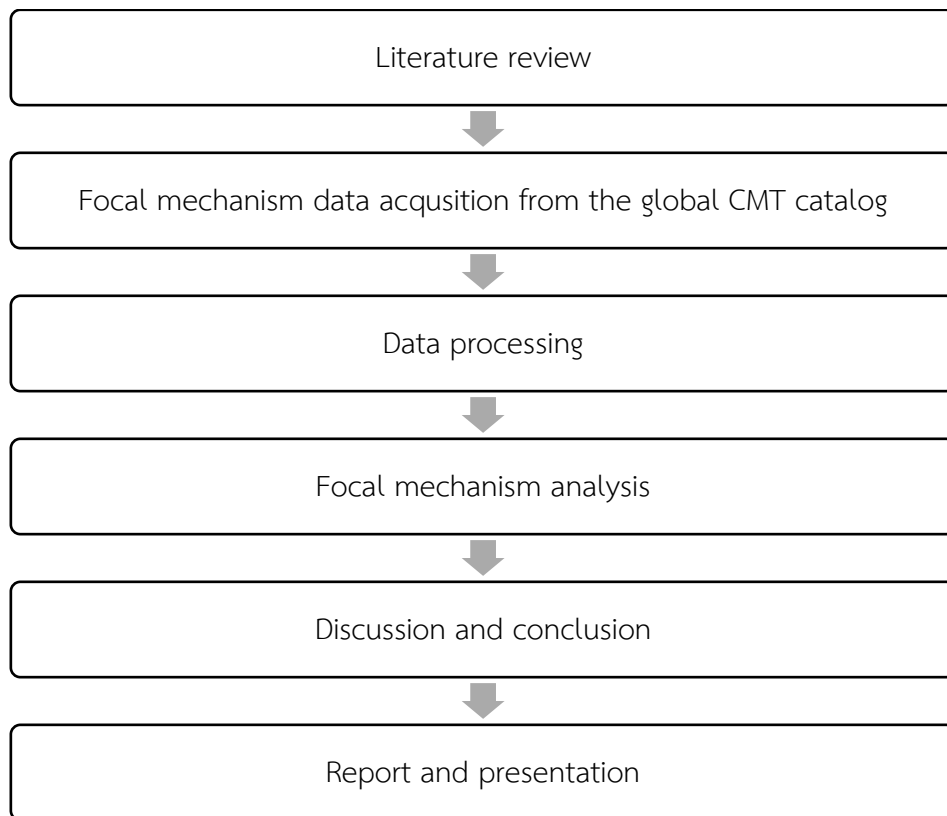


Figure 2.16. Work flow chart.

CHAPTER 3

DATA AND STATISTIC

3.1. Data

Nowadays, earthquake information as well as FMS are opened to the publics. These data are published in many research organization catalogues, such as the Global CMT (GCMT) catalogue, International Seismological Center (ISC), and many local catalogues. In this study, FMSs are retrieved from the GCMT.

The centroid-moment-tensor method is based on the linear relationship between six elements of earthquake moment tensor and the ground motion generated by the earthquake. The regular CMT analysis of earthquakes is originated 2-3 months after the events and completed within 4th month (Elström et al., 2012). However, the GCMT also provides rapid determination of earthquakes with $M_w > 5.5$ and publishes the results in 'quick CMTs' catalogue. The systematic determination started with selecting the earthquakes with $M_w > 5.0$ which have the potential to yield robust centroid-moment-tensor results. For each event, waveform data from seismic stations around the world are retrieved and selected using an aid from automatic waveform selection software. After that, an initial moment-tensor inversion is performed then the automatic-editor software is used to improve the selection. The inversion and reselection are performed again and again until the result does not improve. Usually, the automatic approach of an individual earthquake repeats six times before a human analyst inspects the results. Only acceptable results determined by one of the principal investigators of the project are added to the online GCMT catalogue (www.globalcmt.org).

The GCMT results contain all of the information and FMS of an earthquake, as well as the uncertainty values of each parameter (Figure 3.2). In this study, the data used are event date, original time, location of the epicenter, focal depth, magnitude (M_w), and nodal plane orientations and slip motions. The parameters used to search the catalogue are listed below:

Starting date: Year: 1976, Month: 1, Day: 1

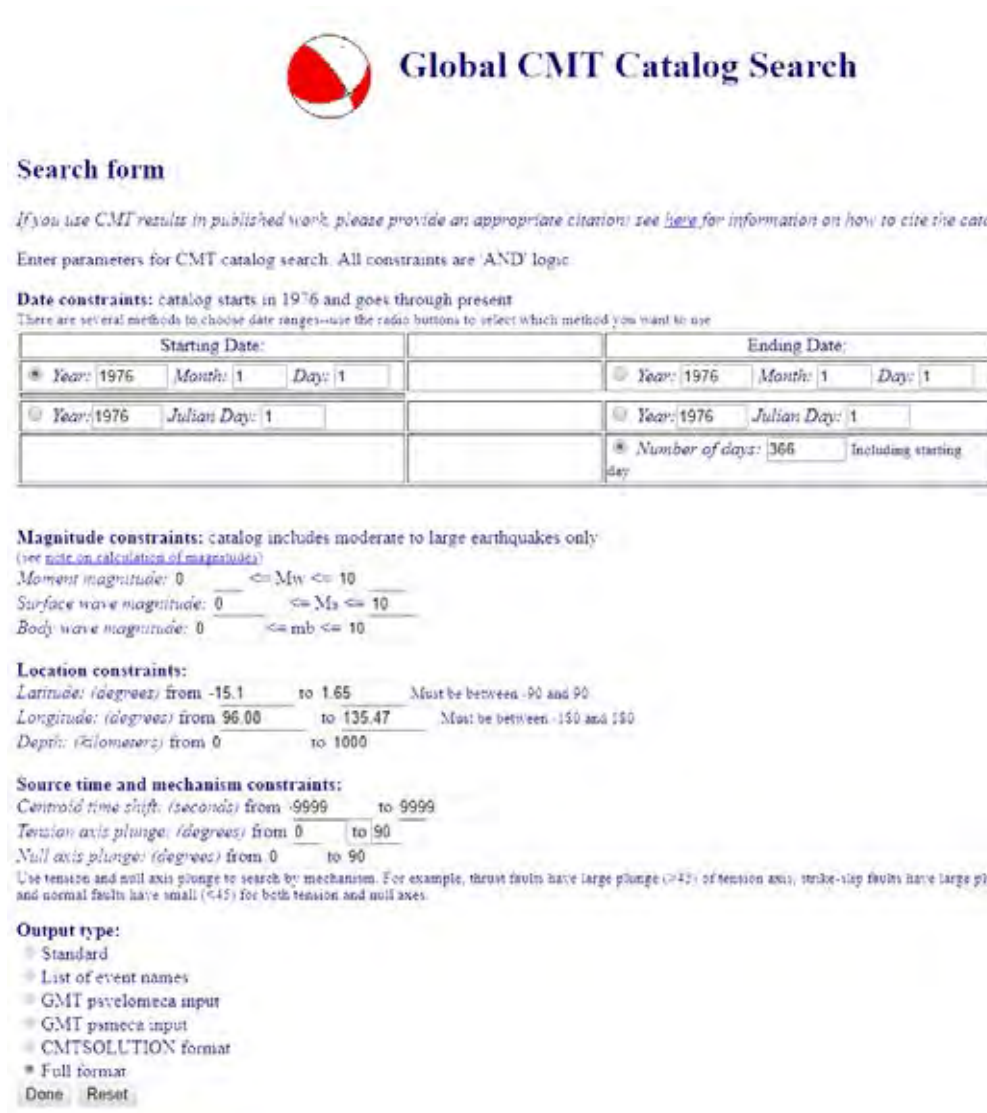
Ending date: Year: 2017, Month: 8, Day, 31


Latitude (degrees) from: -15.1, to: 1.65

Longitude (degrees) from: 96.08, to: 135.47

Output type: Full format

For other parameters, leave them as defaults.



 **Global CMT Catalog Search**

Search form

If you use CMT results in published work, please provide an appropriate citation; see [here](#) for information on how to cite the catalog. Thanks!

Enter parameters for CMT catalog search. All constraints are 'AND' logic.

Date constraints: catalog starts in 1976 and goes through present
There are several methods to choose date ranges—use the radio buttons to select which method you want to use

Starting Date:			Ending Date:		
<input checked="" type="radio"/> Year: 1976	Month: 1	Day: 1	<input type="radio"/> Year: 1976	Month: 1	Day: 1
<input type="radio"/> Year: 1976	Julian Day: 1		<input type="radio"/> Year: 1976	Julian Day: 1	
			<input checked="" type="radio"/> Number of days: 366	Including starting day	

Magnitude constraints: catalog includes moderate to large earthquakes only
(see [note on calculation of magnitudes](#))
Moment magnitude: 0 ≤ Mw ≤ 10
Surface wave magnitude: 0 ≤ Ms ≤ 10
Body wave magnitude: 0 ≤ mb ≤ 10

Location constraints:
Latitude (degrees) from -15.1 to 1.65 Must be between -90 and 90
Longitude (degrees) from 96.08 to 135.47 Must be between -180 and 180
Depth (kilometers) from 0 to 1000

Source time and mechanism constraints:
Centroid time shift (seconds) from -9999 to 9999
Tension axis plunge (degrees) from 0 to 90
Null axis plunge (degrees) from 0 to 90
Use tension and null axis plunge to search by mechanism. For example, thrust faults have large plunge (>45°) of tension axis, strike-slip faults have large plunge of null axis, and normal faults have small (<45°) for both tension and null axes.

Output type:

- Standard
- List of event names
- GMT psvelomeca input
- GMT psmeca input
- CMTSOLUTION format
- Full format

Done Reset

Figure 3.1. The GCMT catalogue search (<http://www.globalcmt.org/CMTsearch.html>).

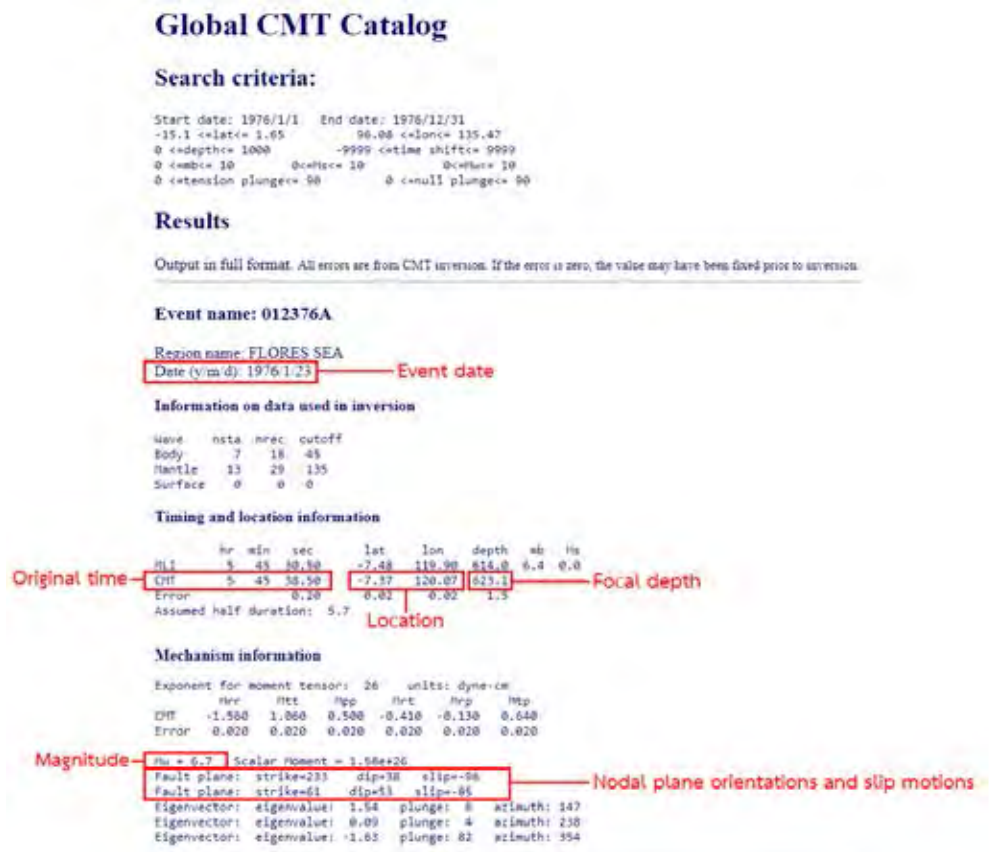


Figure 3.2. Example of the focal mechanism data in GCMT catalogue. The information inside red rectangles are the ones used in this study.

The total number of FMS data retrieved from the GCMT catalogue is 3,842 events. After acquire data from the catalogue, unrelated events are filtered out. The actual data studied in this research are total of 2,998 events, ranging from 23 Jan 1976 to 29 Mar 2017 (Figure 3.3).

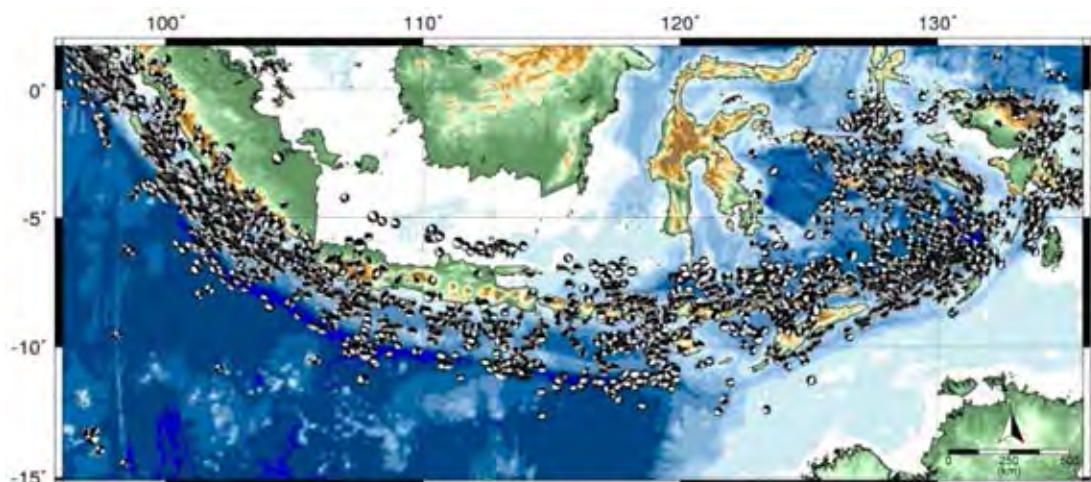


Figure 3.3. Map showing the distribution of all 2,998 FMS data used in this study.

Table 3.1. FMS of the largest earthquakes ($M_w > 7.0$) in the study area.

Lon	Lat	Y	M	D	Hr	Min	Dep	Mw	Str1	Dip1	Rake1	Str2	Dip2	Rake2
118.23	-11.14	1977	8	19	6	9	23	8.3	260	24	-73	61	67	-98
125.72	-7.92	1977	8	27	7	12	20	7	249	46	113	38	49	68
107.68	-11.26	1979	7	24	19	31	20	7	65	46	-180	334	90	-44
125.99	-7.28	1982	6	22	4	18	473	7.4	354	41	-140	232	65	-56
128.32	-7.44	1983	11	24	5	30	157	7.4	74	39	59	291	57	113
97.84	-0.23	1984	11	17	6	49	25	7.1	334	10	116	128	81	86
134.71	-1.63	1985	11	17	9	40	13	7.1	179	64	174	271	85	26
131.20	-5.53	1987	6	17	1	32	75	7.1	305	50	142	62	62	47
120.95	-7.30	1990	5	24	10	9	580	7.0	46	25	-107	245	66	-82
122.49	-8.34	1992	12	12	5	29	20	7.7	80	40	95	253	50	86
130.52	-6.60	1992	12	20	20	52	70	7.2	89	53	37	335	61	137
113.04	-11.03	1994	6	2	18	17	15	7.8	278	7	89	99	83	90
129.65	-6.93	1995	12	25	4	43	161	7.0	277	47	144	33	64	49
123.02	-7.38	1996	6	17	11	22	584	7.8	225	50	-131	98	54	-52
128.95	-6.94	1998	11	9	5	38	25	7.0	289	37	111	84	56	75
125.00	-2.03	1998	11	29	14	10	16	7.7	92	63	-28	196	67	38
101.94	-4.73	2000	6	4	16	28	44	7.8	92	55	152	199	67	38
97.17	-13.47	2000	6	18	14	44	15	7.3	315	16	103	121	85	-153
102.36	-5.40	2001	2	13	19	28	21	7.3	315	16	103	121	74	86
134.30	-1.79	2002	10	10	10	50	15	7.5	60	83	4	329	86	173
134.78	-4.03	2004	2	7	2	42	12	7.3	261	68	-7	354	83	-158
104.38	-2.68	2004	7	25	14	35	600	7.3	108	45	-129	337	56	-57
125.12	-7.87	2004	11	11	21	26	17	7.5	67	27	72	267	65	99
129.99	-6.54	2005	3	2	10	42	196	7.1	308	35	176	41	88	55
128.20	-5.61	2006	1	27	16	58	397	7.6	43	42	-44	169	63	-123
107.78	-10.28	2006	7	17	8	19	20	7.7	290	10	102	98	80	88
107.58	-6.03	2007	8	8	17	4	305	7.5	330	30	155	82	78	62
100.99	-3.78	2007	9	12	11	10	24	8.5	328	9	114	123	82	86
100.13	-2.46	2007	9	12	23	48	43	7.9	317	19	102	125	71	86
99.36	-2.31	2007	9	13	3	35	17	7.0	312	10	90	132	80	90
99.95	-2.66	2008	2	25	8	36	14	7.2	317	6	102	124	84	89
132.83	-0.38	2009	1	3	19	43	15	7.7	99	23	47	324	73	106
133.48	-0.58	2009	1	3	22	33	18	7.4	101	26	72	300	66	98
107.33	-8.12	2009	9	2	7	55	53	7.0	54	46	117	198	50	65
99.67	-0.79	2009	9	30	10	16	78	7.6	74	52	139	193	58	46
133.78	-4.92	2010	9	29	17	11	18	7.0	185	43	-75	345	49	-104
99.32	-3.71	2010	10	25	14	42	12	7.8	316	8	96	130	82	89
129.83	-6.65	2012	12	10	16	53	159	7.1	309	48	166	48	80	43
122.50	-7.35	2015	2	27	13	45	552	7.0	38	51	-14	137	76	-141

3.2. Seismotectonic Setting

3.2.1. Terminology

The relationship between lithospheric plates plays a major role in seismic activities at the plate boundaries. For example, the earthquake rate is high where the plates moving away from each other, but those earthquakes are shallow and small. In the area where plates move pass each other, shallow earthquakes with various magnitude can be found. Converging movement of the plates, especially collision and subduction, can cause large earthquakes. The earthquakes occurring at the convergent boundaries can be divided into 3 groups based on their seismotectonic setting (see Figure 3.4):

1.) Interplate earthquakes occur at the plate boundaries. The earthquakes are of shallow depth, usually 12-33 km deep depends on the thickness of the crust. The majority of them are large ones, because they are direct results of plate collision.

2.) Intraplate earthquakes are the earthquakes occur at the faulting within the plate. Alike interplate earthquakes, the focal depths of intraplate earthquake depend on the crust thickness and there are possibilities of high magnitude earthquakes.

3.) Intraslab earthquakes are intermediate to deep focus earthquakes (34-700 km) occurring within the descending slab.

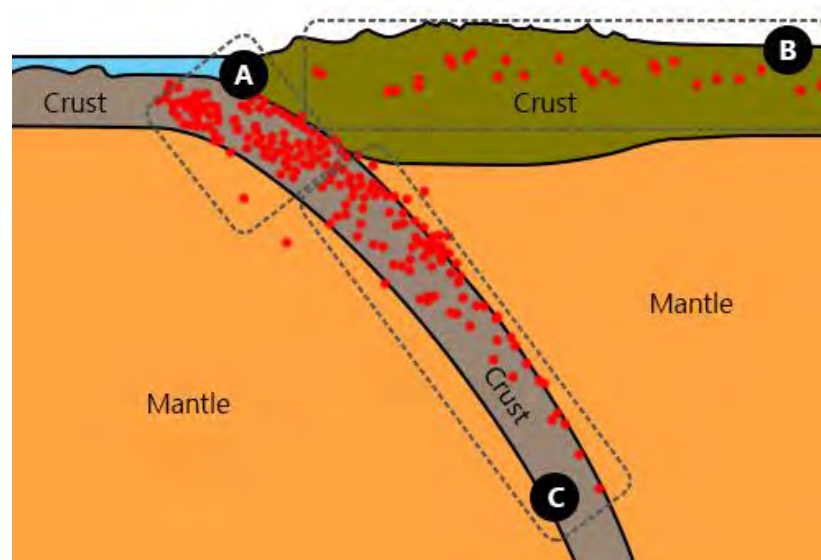


Figure 3.4. Model showing different types of earthquakes in the subduction zone based on their seismotectonic setting. A= interplate earthquakes, B= intraplate earthquakes, C=intraslab earthquakes (Pailoplee, 2018).

3.2.2. Seismotectonic of the Indonesian Archipelago

Charusiri and Pailoplee (2015) has studied the distribution of focal depth in the SSZ and computed 2 cross-sections across the area as shown in Figure 3.5. The section shows the Wadati-Benioff zone in Java area (section 3) and Banda arc (section 4) which can be interpreted that the seismogenic zone in the SSZ spreads to the depth of 40-60 km. The histogram showing the distribution of the focal depth from the data used in this study is generated (Figure 3.6). The graph shows that most of the earthquakes occurred within 0-50 km deep and the frequency decreases exponentially with increasing depth, which agrees with Charusiri and Pailoplee (2015). Hence, in this study, the depth of 50 km is used as the lower limit of the interplate earthquakes. After divided data into 2 categories, interplate earthquakes (1,859 events) and intraslab earthquakes (1,114 events), the maps showing the locations of those earthquakes have been generated and shown in Figure 3.7 and 3.8.

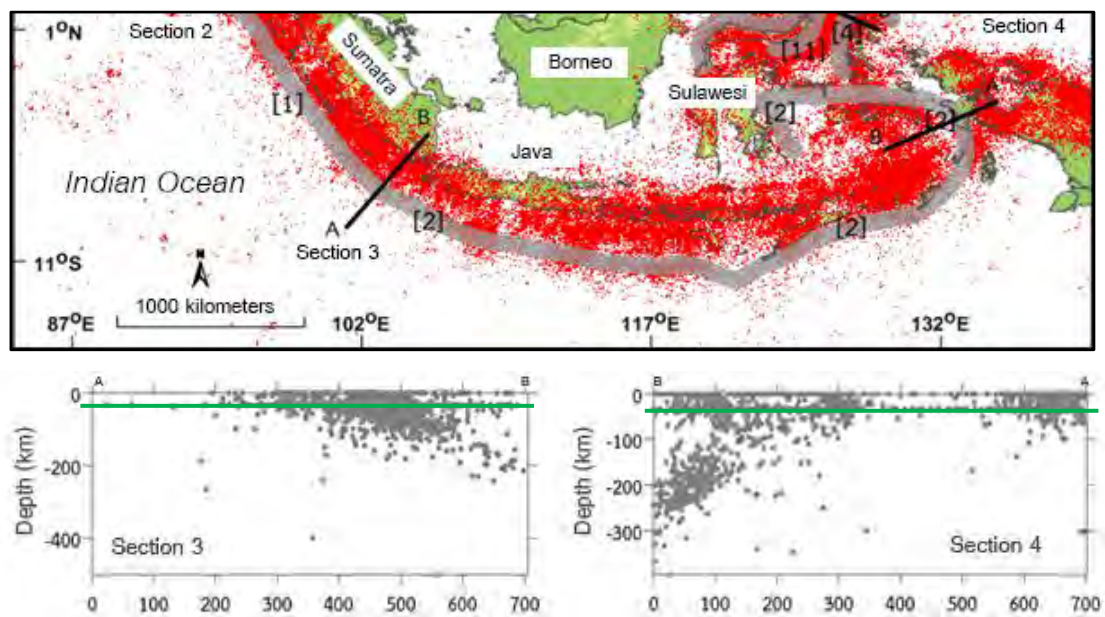


Figure 3.5. Map showing the distribution of the earthquakes in the Indonesian Archipelago. Red dots represent the location of earthquakes. Grey lines show the subduction zone. Section 3 and Section 4 are cross-sections showing the distribution of earthquake (grey dots) in the SSZ. Noted: [1]=Sumatra-Andaman Subduction zone, [2]=Sunda trench, (B) and (C) (Charusiri and Pailoplee, 2015).

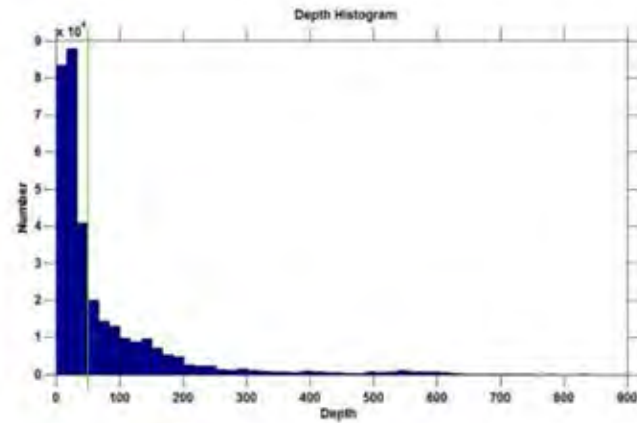


Figure 3.6. Histogram showing distribution of focal depth of earthquakes used in this study. Green line indicates the depth of 50 km which is the cutoff depth separating interplate and intraslab earthquakes.

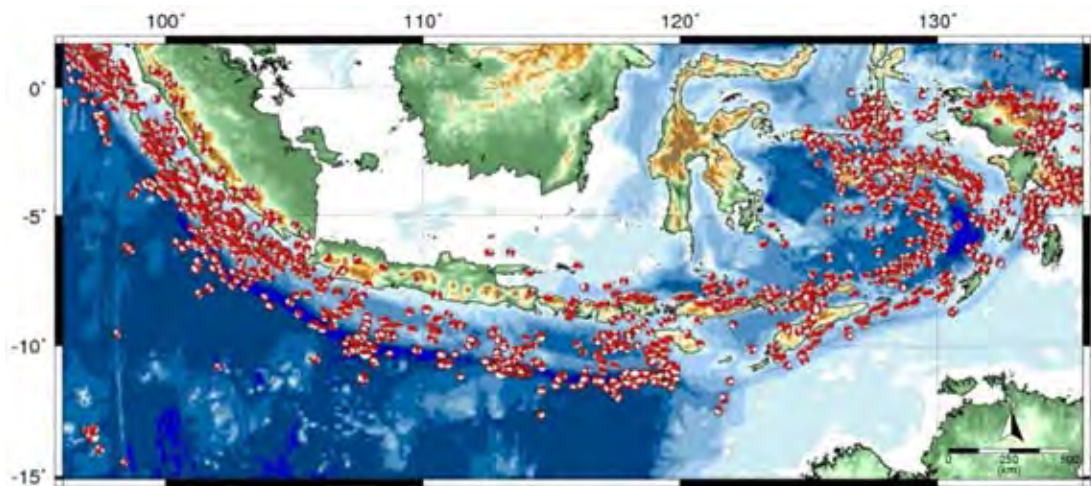


Figure 3.7. Map showing the location and the FMS of the interplate earthquakes.

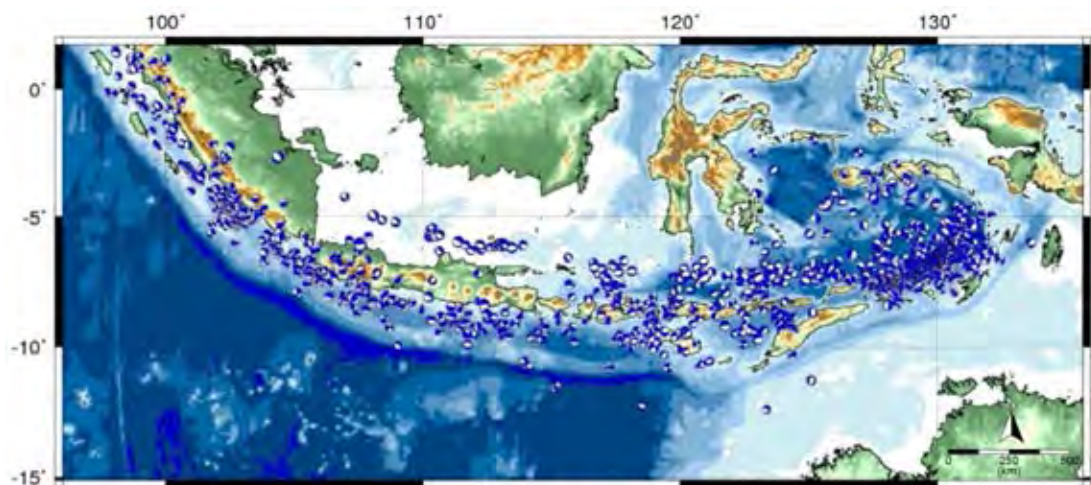


Figure 3.8. Map showing the location and the FMS of the intraslab earthquakes.

3.3. Fault Plane Determination

The FMS acquired from the GCMT catalogue contains 2 set of nodal plane data. In order to use these focal mechanism data for analysis, the actual fault plane must be determined first. For each category, contour maps and rose diagrams of strike, dip, and rake are generated. Other information such as the shape of the subduction zone, and types of faulting in the area are used to help picking up the fault plane data.

3.3.1. Fault plane determination of interplate earthquakes

The contour maps of each parameter of FMS dataset 1 were generated and shown in table 3.2. The rose diagram of strike1 shows that most of faulting oriented in NW direction, which is go with the orientation of the subduction zone. The dip angles of dataset 1 vary between 30° - 45° with the average of 40° . The rake angles of dataset 1 are clustered and show reverse faulting mechanism.

The contour maps of each parameter of FMS dataset 2 were generated and shown in table 3.3. The rose diagram of strike2 shows that most of faulting oriented in SE direction. The dip angles of dataset 2 vary between 45° - 90° with an average of 69.5° . The rake angles of dataset 2 are clustered and show reverse faulting mechanism.

In this study, the dataset 1 was chosen for further analysis as the strike 1 is in line with the pre-existing subduction zone orientation.

Table 3.2. Contour maps and rose diagrams showing the distribution of each FMS parameter of interplate earthquakes' nodal plane 1.

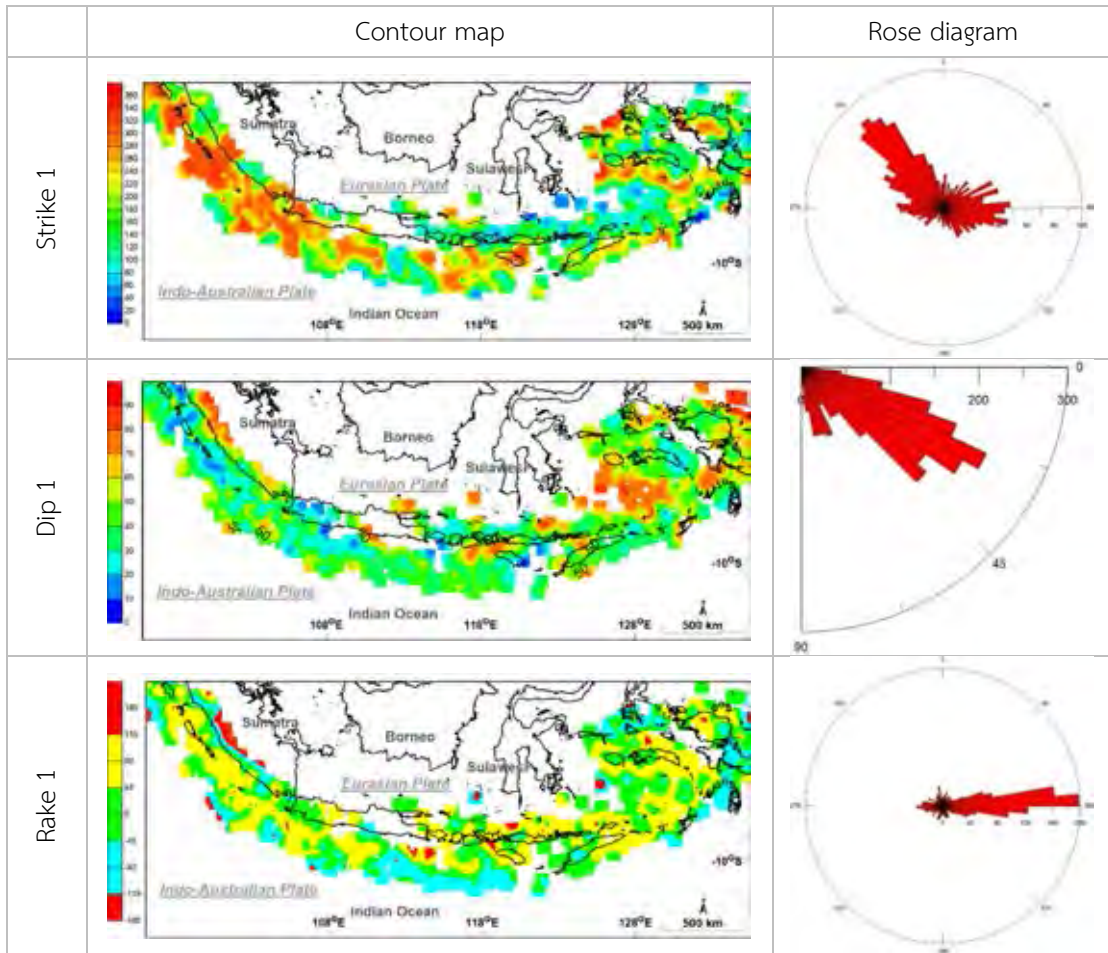
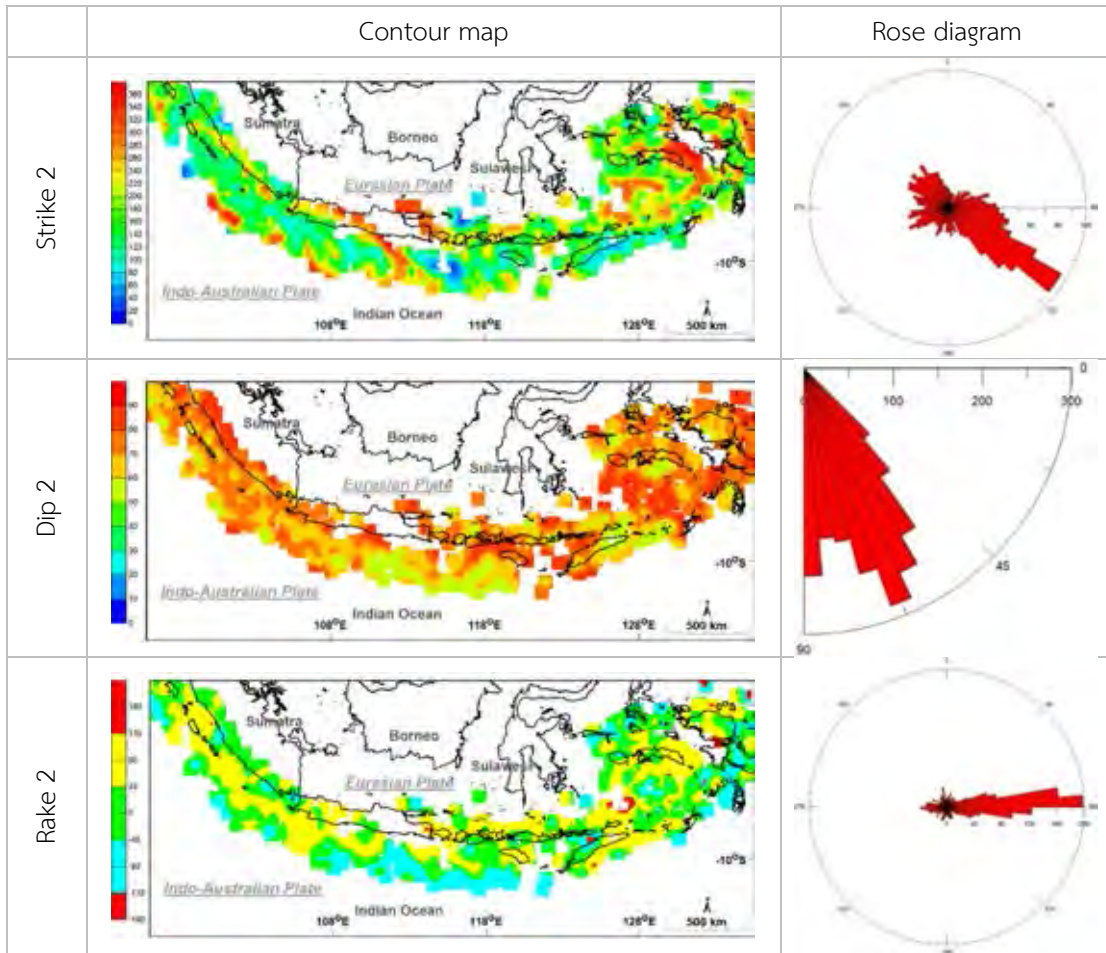


Table 3.3. Contour maps and rose diagrams showing the distribution of each FMS parameter of interplate earthquakes' nodal plane 2.



3.3.2. Fault plane determination of intraslab earthquakes

The contour maps of each parameter of FMS dataset 1 were generated and shown in table 3.4. The rose diagram of strike1 shows various strike. The dip angles of dataset 1 vary between 30°-60° with the average of 40°. The rake angles of dataset 1 are various and most are reverse and strike-slip faulting mechanism.

The contour maps of each parameter of FMS dataset 2 were generated and shown in table 3.5. The rose diagram of strike2 shows that strikes are clustered in 2 directions, most are between 40°-135° and a few between 225°-320°. The dip angles of dataset 2 vary between 45°-90° with an average of 68.5°. The rake angles of dataset 2 are clustered and dominated with reverse faulting mechanism.

In this study, the dataset 1 was chosen for further analysis as the FMS goes along with the pre-existing subduction zone orientation.

Table 3.4. Contour maps and rose diagrams showing the distribution of each FMS parameter of intraplate earthquakes' nodal plane 1.

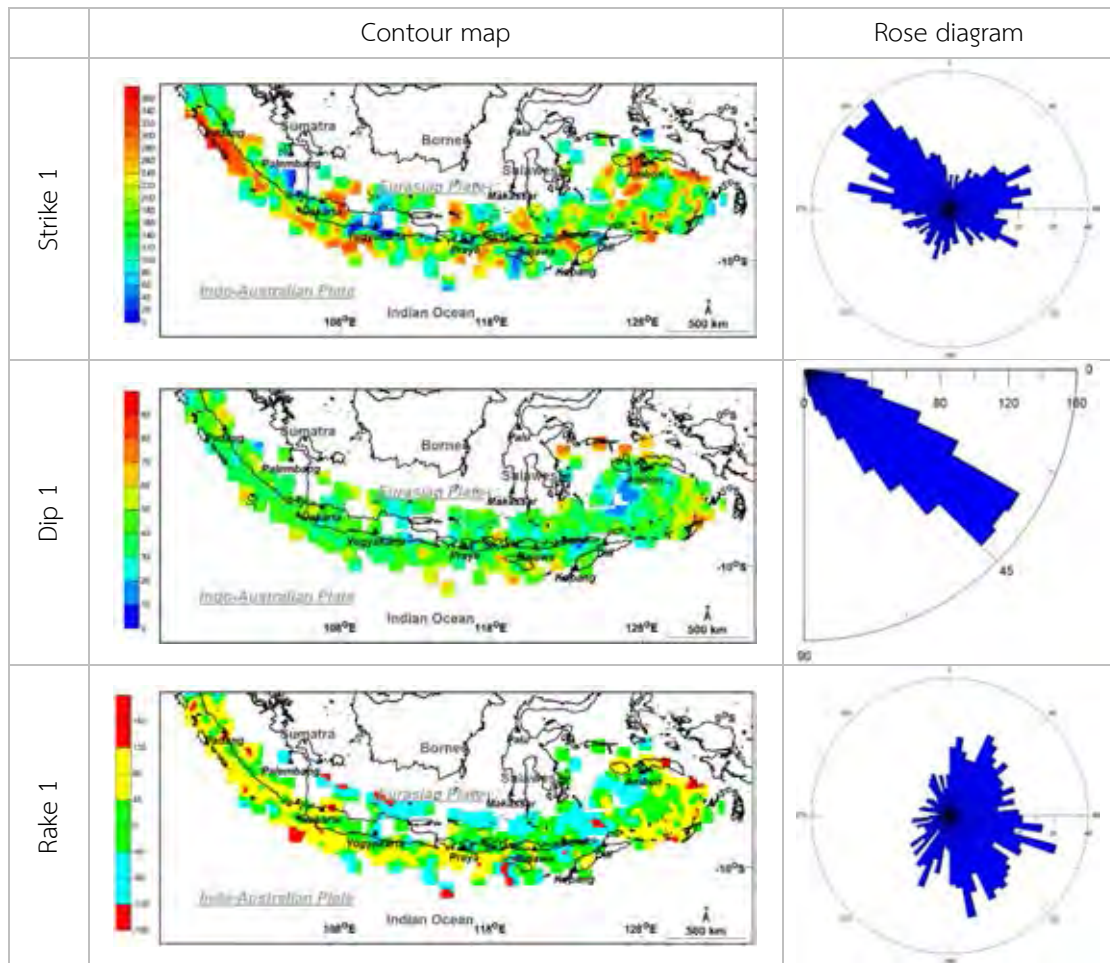
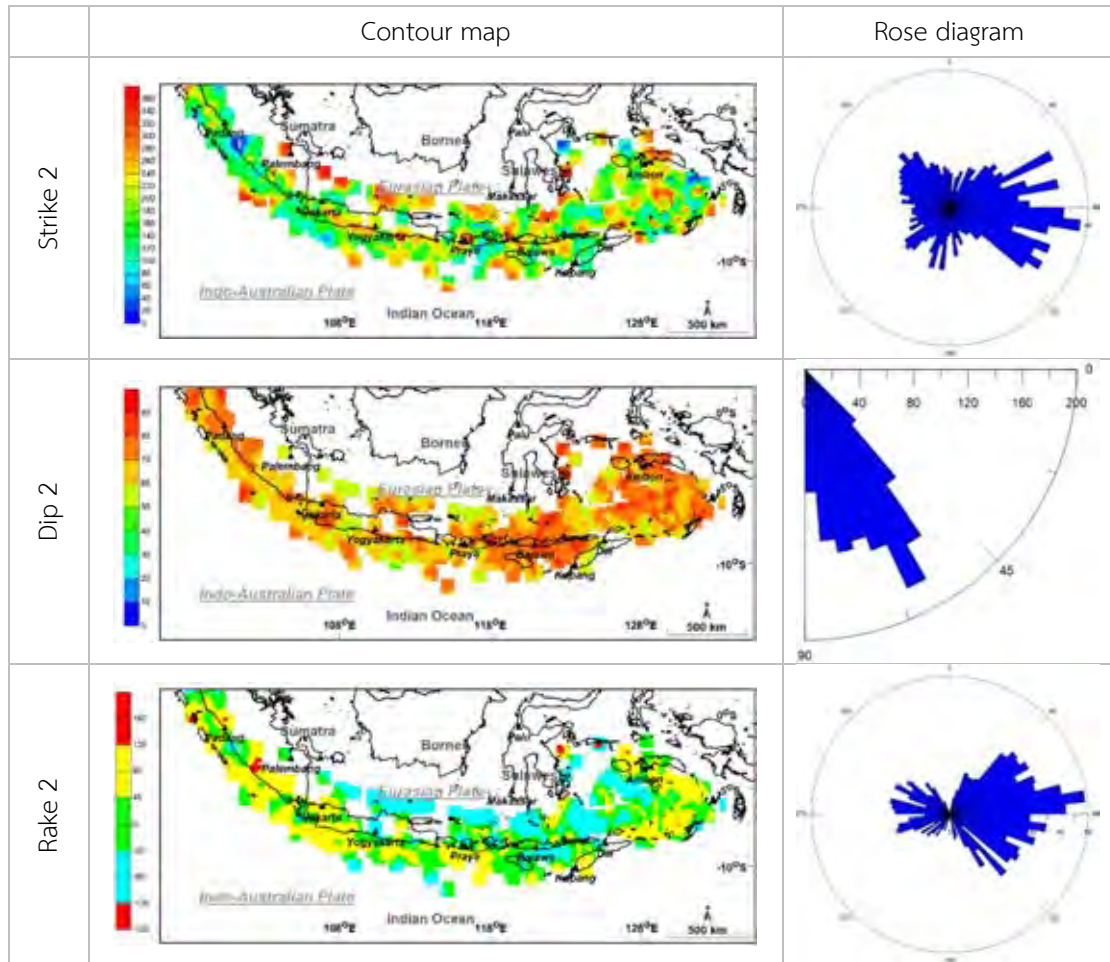


Table 3.5. Contour maps and rose diagrams showing the distribution of each FMS parameter of intraplate earthquakes' nodal plane 2.



CHAPTER 4

FOCAL MECHANISMS ALONG THE INDONESIAN ARCHIPELAGO

4.1. Focal Mechanism of the Study Area

The ternary diagram (Figure 4.1) of all events shows diverse FMS. The majority of the earthquakes in the area are reversed faulting which is consistent to the subduction zone tectonic setting. Apart from reversed faulting, the area has significant number of strike-slip faulting. It could be related to oblique subduction or difference subduction rate along the subduction zone. Normal faulting also significantly present in the area. The pressure and tension axes (Figure 4.2) show that the area as a whole is under compressional regime with NNE-SSW sub-horizontal P-axes and sub-vertical T-axes.



Figure 4.1. Ternary diagram showing the distribution of faulting mechanisms of all events. The classification is based on Frohlich and Anderson (1992).

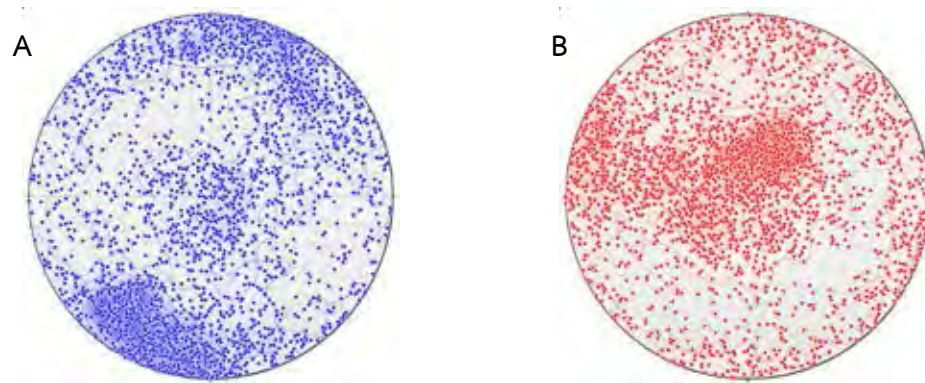


Figure 4.2. Contour map of (A) P-axes (B) T-axes of all events.

4.2. Focal Mechanism of Interplate Earthquakes

The ternary diagram (Figure 4.3) of interplate earthquakes shows diverse FMS. The majority of the earthquakes in the area are reversed faulting which is consistent to the subduction zone tectonic setting. There are also significant numbers of strike-slip faulting and normal faulting. The area is experiencing NNE-SSW compression (Figure 4.4). Most of P-axes are sub-horizontal while some axes are vertical (the cluster at the center of the Figure 4.4 (A)). T-axes are pretty diffused over the map with the majority clustered at the center showing almost vertical orientations.

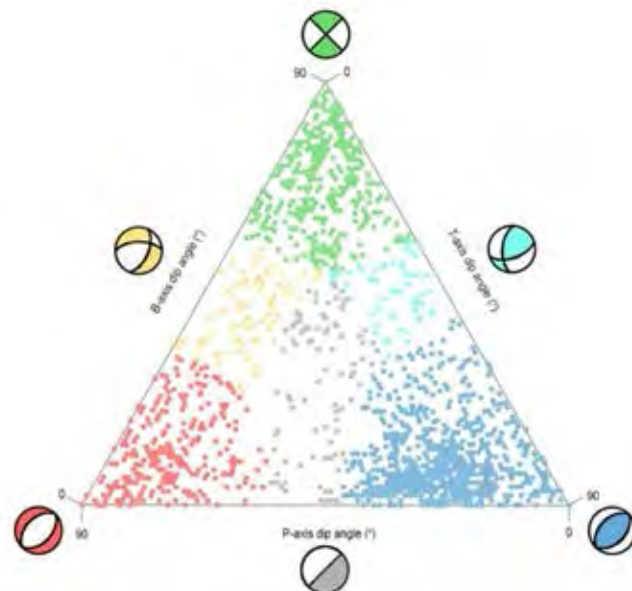


Figure 4.3. Ternary diagram showing the distribution of faulting mechanisms of interplate earthquakes. The classification is based on Frohlich and Anderson (1992).

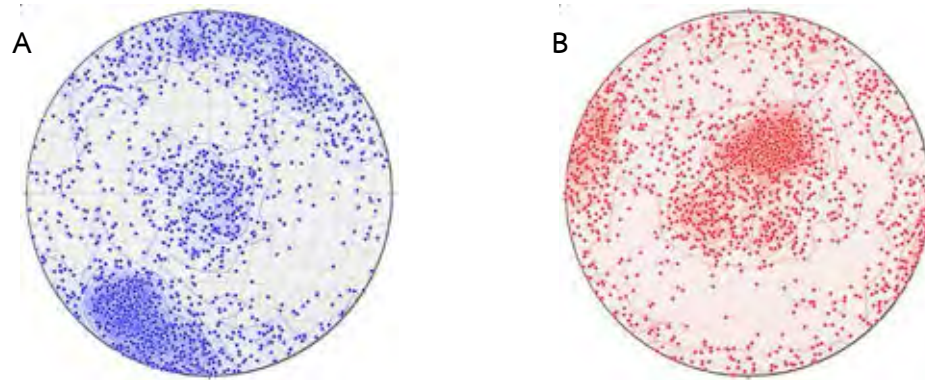


Figure 4.4. Contoured map of (A) P-axes (B) T-axes of interplate earthquakes.

The area can be divided into 12 sub-regions based on the homogeneity of the FMS (Figure 4.5). For each sub-region, the contoured pressure and tension axes (P-T axes) map and ternary diagram were produced to evaluate the variations among the sub-regions, then an average focal mechanism of each sub-region was computed (Table 4.1). From the FMS, the area is dominated by reversed faulting mechanism with 6 sub-regions showing the particular solution. All of them are located along the subduction zone or backarc thrust zone. However, 4 sub-regions show strike-slip faulting mechanism and 2 shows normal faulting mechanism. The contoured P-T maps of sub-region S1, S4, S5, S6, S8, and S10 (Offshore Sumatra-Java, Bali-Sumba, Flores Sea, Timor-Kai, Buru-Seram, and Bird's Head) show sub-horizontal P-axes orientations. All of these sub-regions have vertical to sub-vertical T-axes orientations but the axes in sub-regions S1 are clustered while they are diffused over the map in other sub-regions. From the ternary diagrams, sub-region S1 is dominated by reversed faulting earthquakes with considerable numbers of normal and strike-slip faulting earthquakes. Sub-region S4, S5, S6, and S8 are characterized by mixture of reversed and strike-slip faulting mechanisms while sub-region S10 is dominated by reversed faulting mechanism. Sub-region S2, S7, S9, and S11 (Sumatra, South Banda Sea, Seram Sea, and West Papua) have both sub-horizontal T- and P- axes, except sub-region S9 which has sub-horizontal to vertical P-axes. Both axes in these 4 sub-regions are diffused. Strike-slip faulting predominates sub-region S2 and S7 while the mixture of strike-slip and normal faulting is the characteristic of sub-region S9 and S11. Normal faulting dominates sub-region S3 (Offshore Java) and S12 (Aru). The P- and T- axes in both sub-regions are vertically and horizontally oriented respectively.

Table 4.1. Rake-based ternary plots, contour P-T map, and FMS of each interplate sub-region. Noted: Blue = P-axis, Red = T-axis.

Sub-region	Ternary Diagram	Contoured P-T Map	Focal Mechanism	Fault Plane Solution			
				Fault	Strike	Dip	Rake
S1. Offshore Sumatra-Java (819 events)				1	299.2	19.3	87.7
				2	121.9	70.7	90.8
S2. Sumatra (11 events)				1	149.4	84.9	-177.8
				2	59.2	87.8	174.9
S3. Offshore Java (119 events)				1	82.1	40.6	-98.5
				2	49.9	49.9	97.2

Table 4.1. (Continued) Rake-based ternary plots, contour P-T map, and FMS of each interplate sub-region. Noted: Blue = P-axis, Red = T-axis.

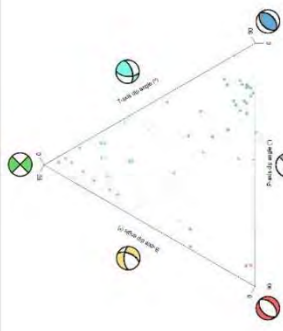
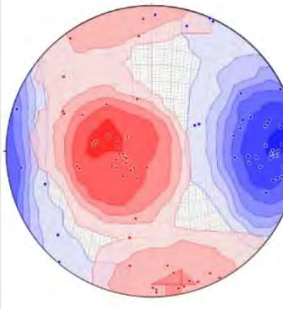
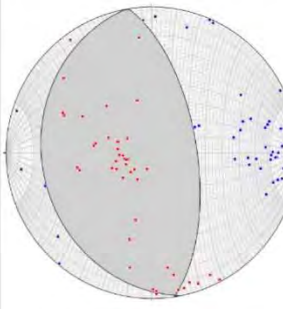
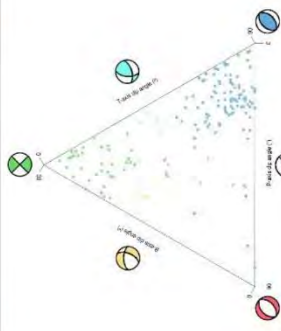
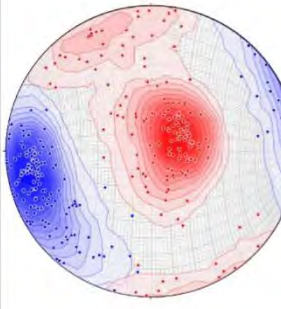
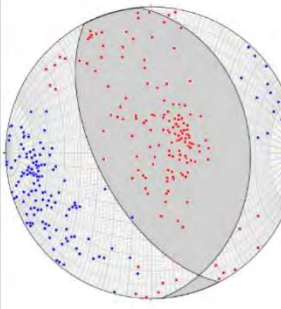
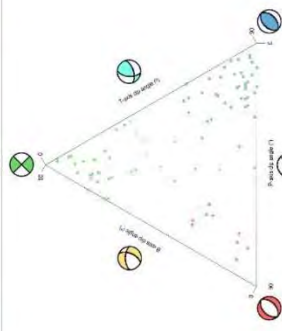
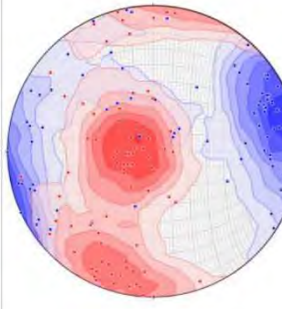
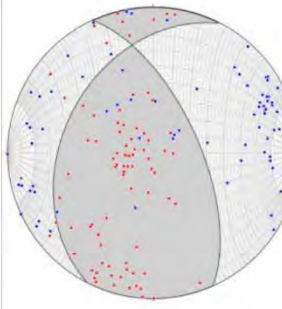
Sub-region	Ternary Diagram	Contoured P-T Map	Focal Mechanism	Fault Plane Solution			
				Fault	Strike	Dip	Rake
S4. Bali-Sumba (55 events)				1	277.2	24	110.9
				2	74.5	67.7	81.0
S5. Flores Sea (172 events)				1	85.9	32.5	110.2
				2	242.4	59.7	77.6
S6. Timor-Kai (84 events)				1	296.9	37.7	134.6
				2	65.7	64.2	61.5

Table 4.1. (Continued) Rake-based ternary plots, contour P-T map, and FMS of each interplate sub-region. Noted: Blue = P-axis, Red = T-axis.

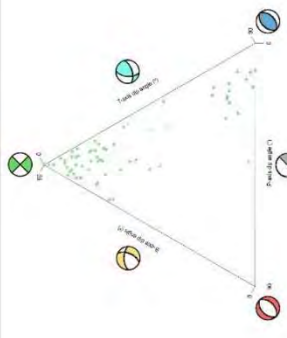
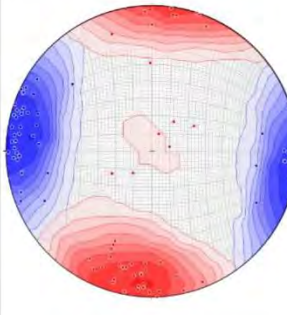
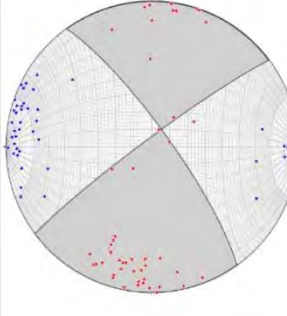
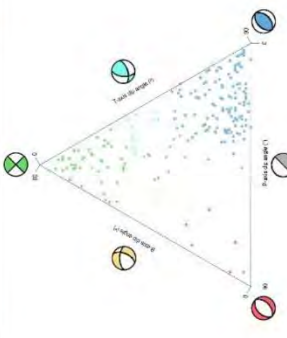
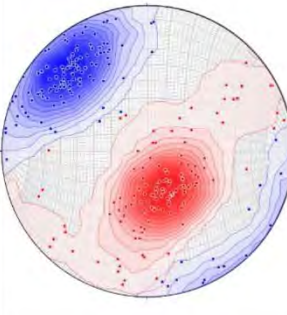
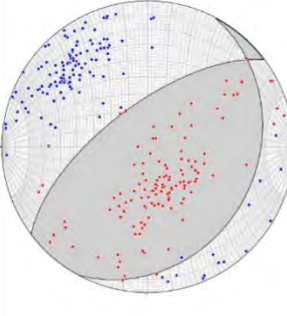
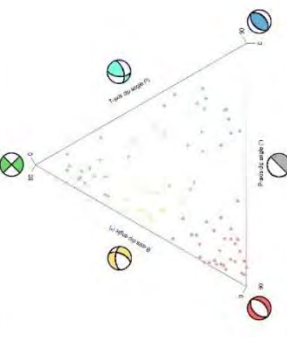
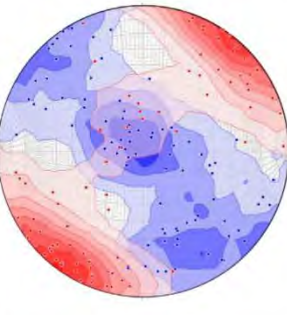
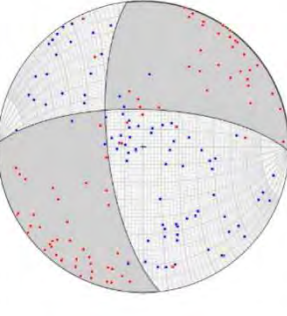

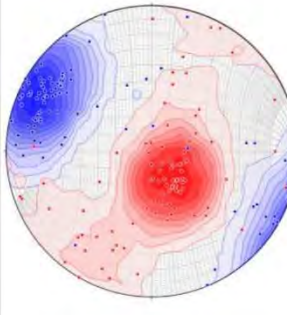
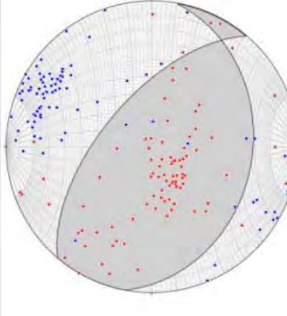
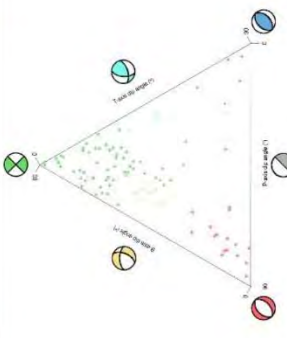
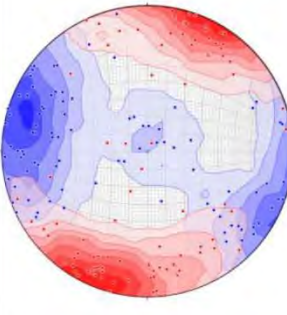
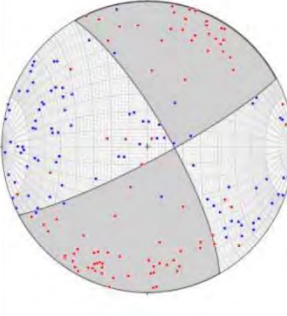
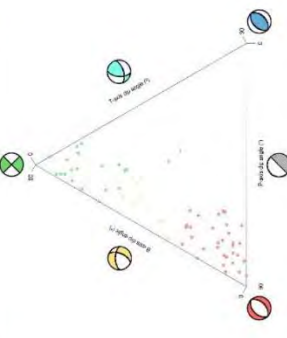
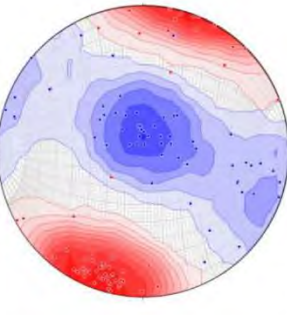
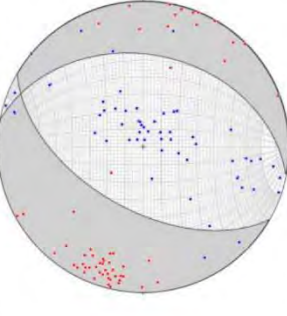
Sub-region	Ternary Diagram	Contoured P-T Map	Focal Mechanism	Fault Plane Solution			
				Fault	Strike	Dip	Rake
S7. South Banda Sea (49 events)				1	54.2	79.8	4.8
				2	323.4	35.8	169.8
S8. Buru-Seram (210 events)				1	100.9	36.3	56.6
				2	320.2	60.4	112.0
S9. Seram Sea (83 events)				1	1.5	68.8	-158.5
				2	263.5	70.0	157.4

Table 4.1. (Continued) Rake-based ternary plots, contour P-T map, and FMS of each interplate sub-region. Noted: Blue = P-axis, Red = T-axis.

Sub-region	Ternary Diagram	Contoured P-T Map	Focal Mechanism	Fault Plane Solution			
				Fault	Strike	Dip	Rake
S10. Bird's Head (92 events)				1	100.2	31.4	63.6
				2	310.3	62.2	105.2
S11. West Papua (92 events)				1	60.3	77.0	-8.0
				2	152.1	82.2	13.1
S12. Aru (59 events)				1	11.0	36.6	-105.5
				2	210.0	54.9	101.2

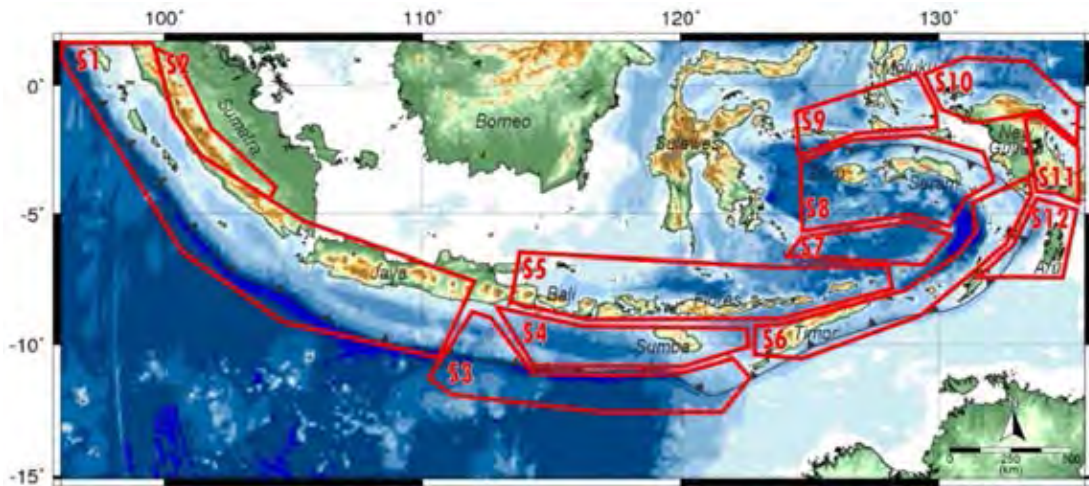


Figure 4.5. Map showing sub-regions of Interplate earthquakes.

4.3. Focal Mechanism of Intraslab Earthquakes

The ternary diagram (Figure 4.6) of interplate earthquakes shows diverse FMS. The area is dominated with reversed faulting earthquakes. Additionally, the area has considerable numbers of normal faulting and oblique faulting earthquakes. Reversed faulting earthquake could be found too. From contoured P- and T-axes map (Figure 4.7), the slab is under NNE-SSW compression and sub-vertical extension. Both of the axes are pretty well clustered, which indicates homogeneous stress field in the area.

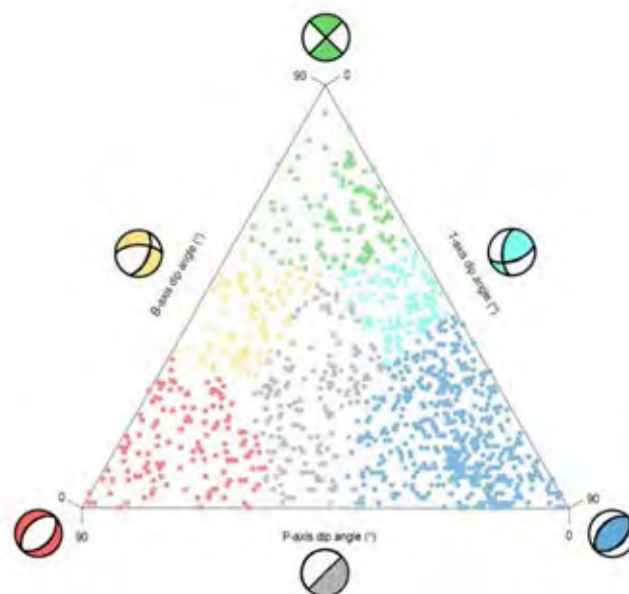


Figure 4.6. Ternary diagram showing the distribution of faulting mechanisms of intraslab earthquakes. The classification is based on Frohlich and Anderson (1992).

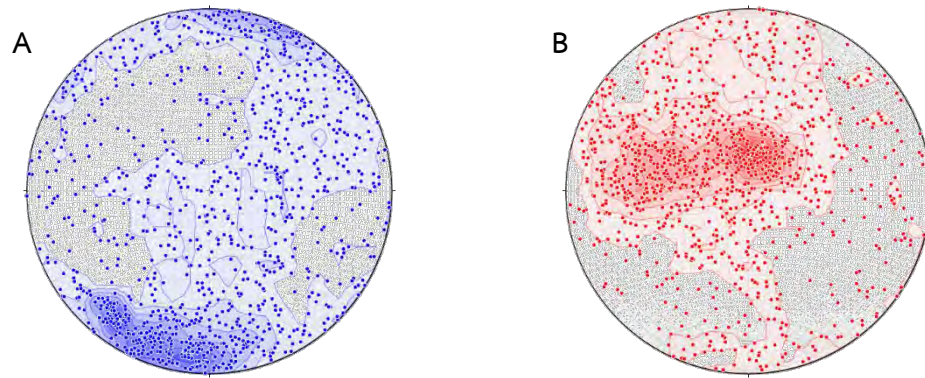


Figure 4.7. Contour map of (A) P-axes (B) T-axes of intraslab earthquakes.

The area can be divided into 5 sub-regions as shown in Figure 4.8. For each sub-region, the contoured P-T axes map, ternary diagram, and average focal mechanism of each sub-region were produced (Table 4.2). From the FMS, the faulting mechanisms are uniform along the whole SSZ with reversed faulting at the shallower depth and normal faulting at the deeper depth with exception of sub-region D3 which show normal faulting mechanism at the shallower depth. Sub-region D1 (Sumatra-Sumbawa) is predominated by compressional faulting mechanisms. The contoured P-T map of sub-region D1 shows sub-vertical T-axes orientation and sub-horizontal P-axes orientation, both of which are slightly clustered. Sub-region D2 (Java Sea) and D4 (Banda Sea) are nominated by normal faulting and have horizontal T-axes orientations. P-axes is vertical in sub-region D2 while in sub-region D4, the axes are inclined and diffused over the stereonet. Sub-region D3 (Sumba-Flores-Timor) has inclined P- and T-axes orientations and both axes are diffused over the contoured map. The region has mixture of all faulting mechanisms.

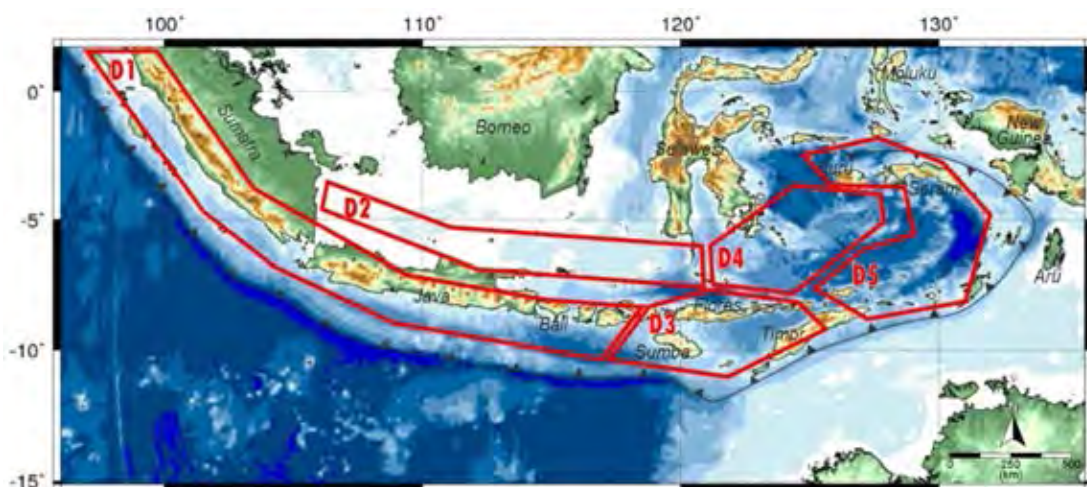


Figure 4.8. Map showing sub-regions of Intraslab earthquakes.

Table 4.2. Rake-based ternary plots, contour P-T map, and FMS of each intraslab sub-region. Noted: Blue = P-axis, Red = T-axis.

Sub-region	Ternary Diagram	Contoured P-T Map	Focal Mechanism	Fault Plane Solution			
				Fault	Strike	Dip	Rake
D1. Sumatra-Sumbawa (341 events)				1	273.7	27.9	75.8
				2	109.6	63.0	97.4
D2. Java Sea (58 events)				1	99.9	41.2	-99.0
				2	291.8	49.4	97.8
D3. Sumba-Flores-Timor (101 events)				1	70.7	17.1	-57.6
				2	217.1	75.6	80.6

Table 4.2. (Continued) Rake-based ternary plots, contour P-T map, and FMS of each intraslab sub-region. Noted: Blue = P-axis, Red = T-axis.

Sub-region	Ternary Diagram	Contoured P-T Map	Focal Mechanism	Fault Plane Solution			
				Fault	Strike	Dip	Rake
D4. Banda Sea (94 events)				1	213.8	41.1	-123.8
				2	75.4	56.8	115.9
D5. Banda Arc (482 events)				1	74.8	53.9	45.3
				2	313.9	54.9	133.9

CHAPTER 5

DISCUSSION AND CONCLUSION

5.1. Interplate Earthquakes

Interplate earthquakes are earthquakes occurring at the boundary between two tectonic plates. In this study, the earthquakes that occurred at the depth of 0-50 km were considered as interplate earthquakes. The area then was divided into 12 sub-regions, and average FMSs for each sub-region were evaluated.

5.1.1. Focal mechanism solutions of interplate earthquakes

Because FMS contains 2 set of nodal planes, the actual fault plane must be determined according to the orientation of the tectonic plates, tectonic setting, and other information. Fault 1 was selected for all sub-regions except sub-region S9 where Fault 2 was selected. The alignment of each of the fault planes are shown in Table 5.1.

Table 5.1. Preferred fault plane orientation and slip rake of interplate earthquakes.

Sub-region	Fault Set	Strike	Dip	Rake
S1. Offshore Sumatra-Java	1	299.2	19.3	87.7
S2. Sumatra	1	149.4	84.9	-177.8
S3. Offshore Java	1	82.1	40.6	-98.5
S4. Bali-Sumba	1	277.2	24	110.9
S5. Flores Sea	1	85.9	32.5	110.2
S6. Timor-Kai	1	296.9	37.3	134.6
S7. South Banda Sea	1	54.2	79.8	4.8
S8. Buru-Seram	1	100.9	36.3	56.6
S9. Seram Sea	2	263.5	70.0	157.4
S10. Bird's Head	1	100.2	31.4	63.6
S11. West Papua	1	60.3	77.0	-8.0
S12. Aru	1	11.0	36.6	-105.5

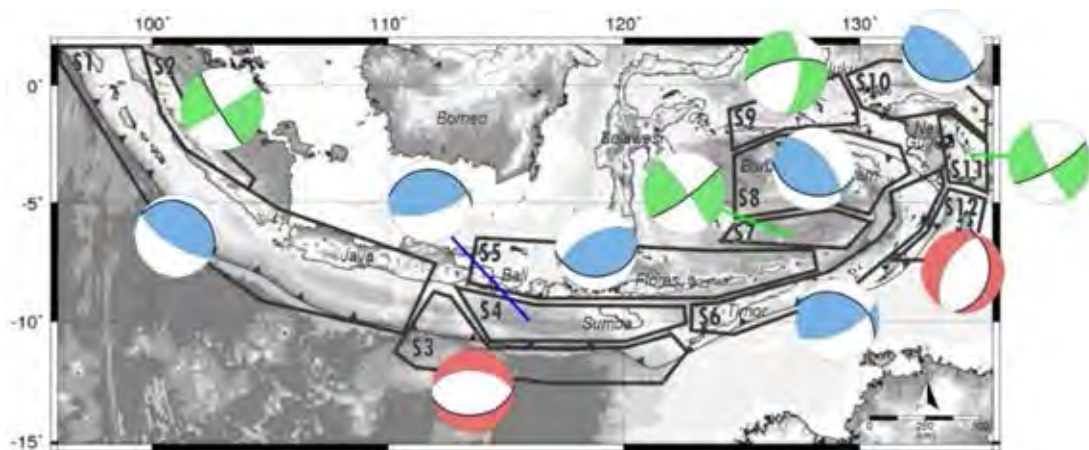


Figure 5.1. Map showing an average focal mechanism of each interplate sub-region. Thick black lines are preferred fault planes. Faulting mechanisms are represented in different colours, red = normal faulting, blue = reversed faulting, green = strike-slip faulting.

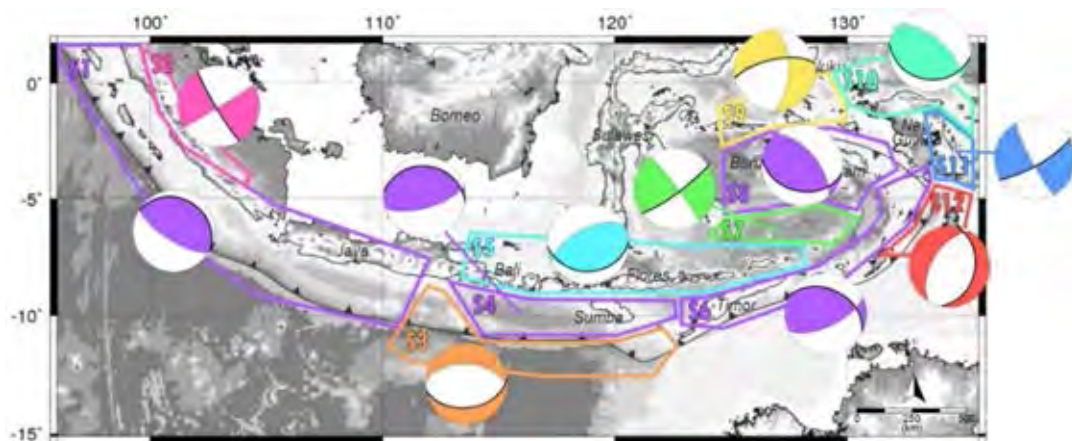


Figure 5.2. Map showing interpret fault zones. Each colour represents each fault zone; purple = the SSZ, pink = the Sumatran Fault Zone, orange = Java-Sumba Outer-rise, Cyan = Flores and Wetar Thrusts, green = South Banda Sea, yellow = Sorong Fault Zone, emerald green = West Papua Subduction, blue = Tarera-Aiduna Fault Zone, red = Aru Trough.

The preferred fault planes and faulting mechanisms are correlated with pre-defined seismic source zones. The interpreted fault zones are shown in Figure 5.2, each colour represents each interpreted fault zone.

The first zone is the SSZ, which is correlate to sub-regions S1, S4, S6, and S8. All of them have reversed faulting mechanism and the strikes parallel to the trend of Sunda Trench. The average dip angles vary from 19.3° in the west to 36.3° in the east. Sub-region S2 is interpreted as the Sumatran Fault Zone, which is right-lateral strike-slip fault. The strike is parallel to the subduction zone and the dip is almost vertical. Noda (2013) classified the Sumatran Fault as a trench-linked strike-slip fault which caused by oblique subduction (Figure 5.3). Sub-region S3 is dominated by normal faulting with strike paralleling to the subduction zone; hence, it can be interpreted as outer-rise region (Figure 5.4). Sub-region S5 shows predominant reversed faulting mechanism. The strike is also parallel to the subduction zone. However, because the sub-region is located at back-arc area, it cannot be grouped with the subduction zone regions, instead, it can be interpreted as back-arc thrust (Figure 5.4). Therefore, sub-region S5 is interpreted as Flores and Wetar Thrust (Figure 5.5).

Sorong Fault Zone and West Papua Subduction (Figure 5.5) coincide with sub-region S9 and S10 respectively. The FMS of West Papua Subduction has the rake angle of 63.6° indicating strike-slip faulting component which might be influenced by Sorong Fault segments that run through Bird's Head Plateau. Tarera-Aiduna Fault Zone can be correlated with sub-region S11. The focal mechanism shows left-lateral strike-slip faulting, with 60° strike though the strike of the fault zone interpreted from surface lineament features is almost E-W (Figure 5.5). This could be because of small NE-SW faults in the sub-regions. The FMS of sub-region 12 show extensive normal faulting mechanism. The strike is almost NNE-SSW and the dip angle is 36.6° . These faults are considered as boundary faults of Aru and Tanimbar Trough as shown in Figure 5.6 (Hall et al., 2017). The extension began in the Late Miocene, as Banda Arc subduction rollback started (Spakman and Hall, 2010).

Sub-region S7 shows strike-slip faulting mechanism. The fault plane solutions show NE-SW striking left-lateral slip and NW-SE striking right-lateral slip. The NW-SE strike coincides with the strike of Lawanopo fault. However, the fault is left-lateral strike-slip fault which goes against the FMS of this sub-region. Hence, the NE-SW striking

fault plane is chosen for this sub-region. Though there is no proposed fault zone in this region, Stanley and Harris (2009) proposed a lineament that stretches from Wetar Thrust in the SW to Tarera-Aiduna Fault in the NE. The lineament also conforms to the trend of earthquake epicenters in South Banda Sea (Figure 5.7). Moreover, the FMS of all earthquakes (51 events) in the region show similar fault plane solutions, with strikes between 40° to 60° , dip angles between 70° - 80° , and rake angles between -25° to 20° . From these evidences, this lineament can be proposed as a new fault zone.

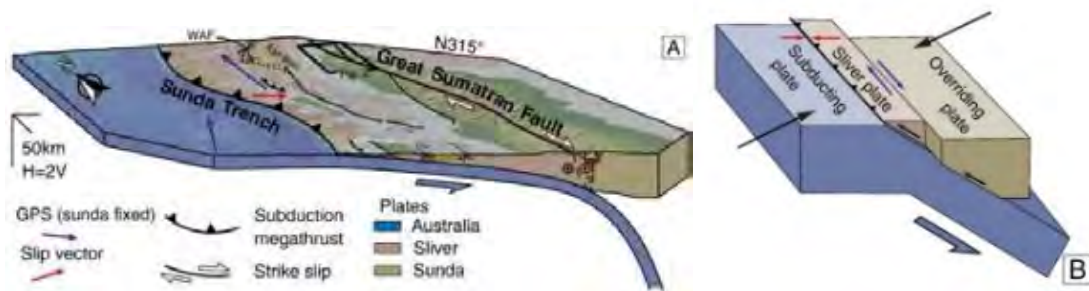


Figure 5.3. Structure and Kinematics of the Great Sumatran Fault Zone. (A) Real-scale 3D view of the tectonic configuration of the northern sector of the Sumatran section of the Sunda arc. (B) Idealized block diagram showing the geometry of the Sliver plate and overall motions under oblique subduction (Fernández-Blanco et al., 2016).

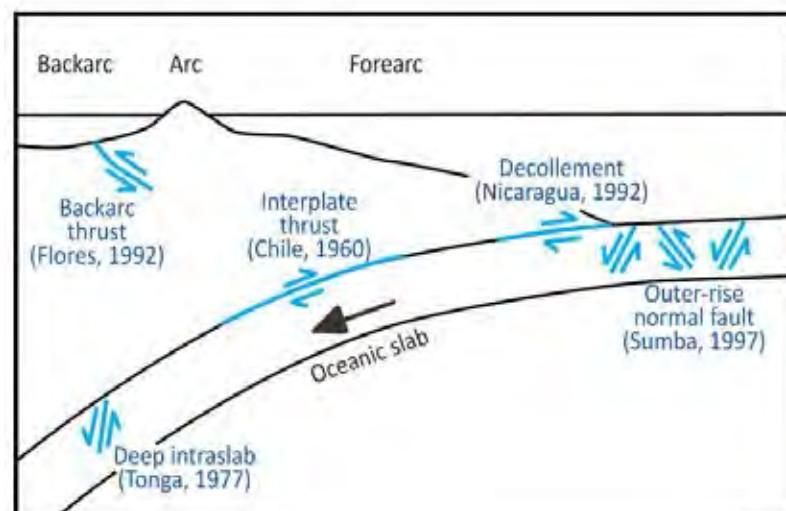


Figure 5.4. Generalized diagram of a subduction zone showing types of fault ruptures (modified from Geist, 1998).

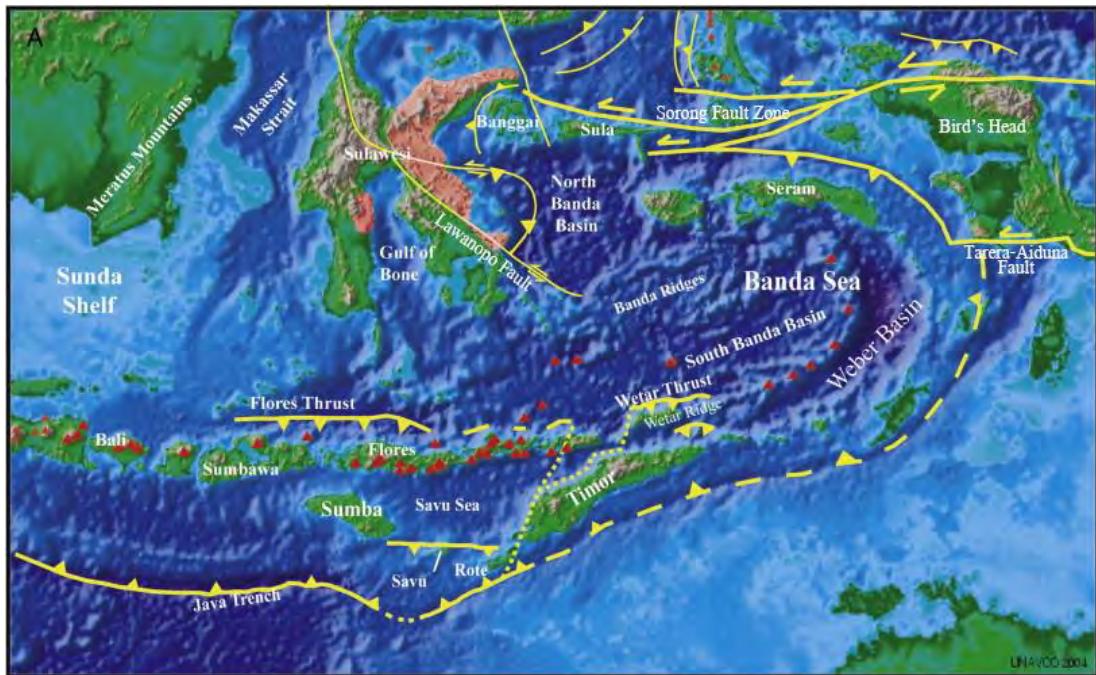


Figure 5.5. Digital elevation model of the Banda Arc region showing active faults (Standley and Harris, 2009).

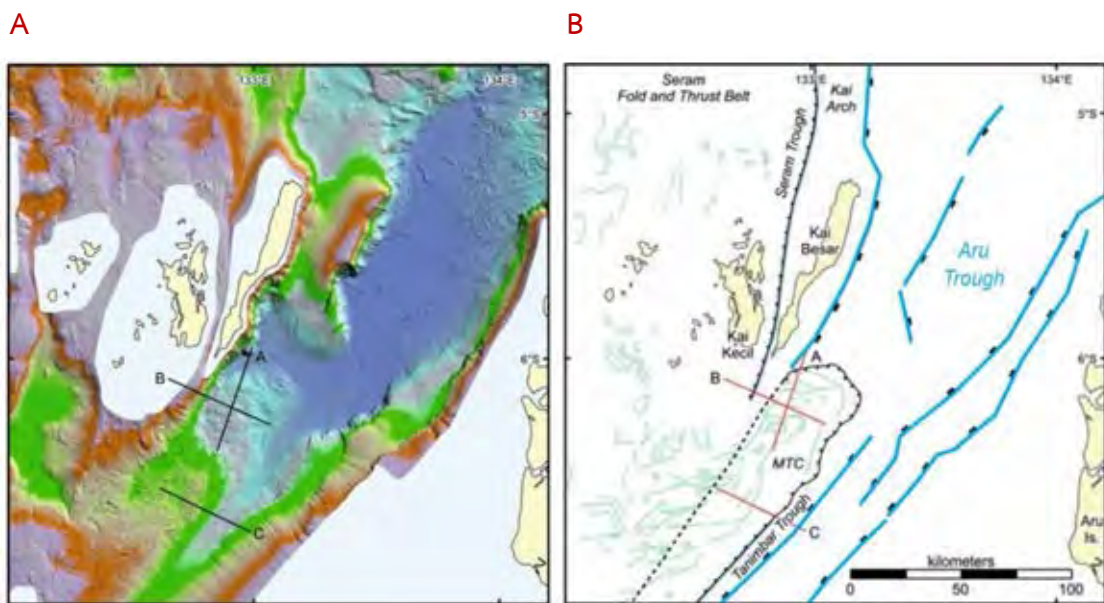


Figure 5.6. Maps showing (A) detailed seafloor bathymetry of Aru Trough, and (B) normal faults that border Aru and Tanimbar Trough (Hall et al., 2017).

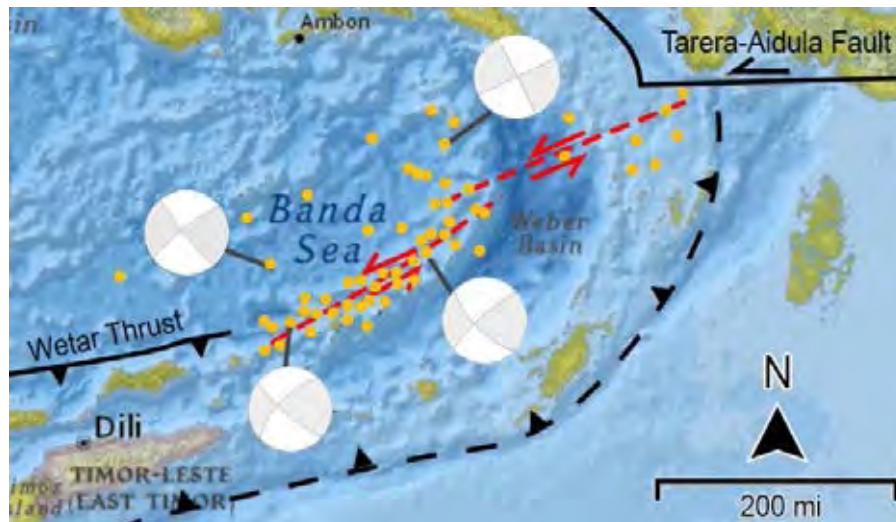


Figure 5.7. Map showing the lineament (red dashed line) that may be responsible for left-lateral strike-slip earthquakes in the South Banda Sea. Orange dots are earthquakes occurring in the region (modified from Standley and Harris, 2009).

5.1.2. Tsunami generation along the Indonesian Archipelago

Indonesian Archipelago has high risk of major tsunami because of the high probabilities of the large underwater earthquakes. However, not all underwater earthquakes are able to trigger tsunamis. There are a few factors controlling tsunami generation; i.e. magnitude, focal depth, and vertical surface displacement. Usually, earthquakes of M_w 7.0 or more release enough energy to generate tsunami (Levin and Nosov, 2016) but not all large earthquakes are capable of tsunami generation. There must be sufficient vertical displacement of the seafloor. For example, a M_w 8.5 strike-slip earthquake is less likely to cause tsunami than M_w 7.0 thrust earthquake.

In order to evaluate the risk of tsunami generation by earthquake along the Indonesian Archipelago, vertical seafloor displacement must be determined first. It has been known that earthquake magnitude may be correlated with rupture parameters (Well and Coppersmith, 1994). Murotani et al. (2013) proposed regression model for large subduction-zone earthquakes as

$$D = 1.66 \times 10^{-7} M_0^{1/3} \quad (1)$$

while D is average slip (m) and M_0 is seismic moment (N.M).

Hans and Kanamori (1979) proposed the relation between seismic moment and moment magnitude (M):

$$\log M_0 = 1.5M + 9.05 \quad (2)$$

The magnitude used in this study is M_w 7.6 as it is the smallest earthquake that may trigger destructive tsunami near the epicenter (U.S. Geological Survey, 2016). The average surface displacement of earthquakes of this magnitude is 1.13 m.

The displacement obtained from the equation (1) is an average displacement on the fault plane in the slip direction, not the vertical surface displacement. To calculate vertical displacement, apart from total slip (displacement on the fault plane), slip rake and dip angle of the fault must be known. From the fault geometry model (Figure 5.8), the dip slip component of rupture can be expressed as

$$u_d = AD \times \sin(\lambda) \quad (3)$$

where u_d is dip-slip component and λ is slip rake.

The vertical displacement is given by

$$VS = u_d \times \sin(\delta) \quad (4)$$

where VS is vertical displacement and δ is dip angle.

Therefore, the relationship between displacement on the fault plane and vertical displacement can be deduced from equation (3) and (4):

$$VS = AD \times \sin(\lambda)\sin(\delta) \quad (5)$$

Then, the vertical seafloor displacement of each interplate sub-region can be evaluate by using equation (4). It is assumed that the surface displacement is depth independent. Noted that sub-region S2 (Sumatra) and S11 (West Papua) are on-land sub-regions so they are opted out for the tsunami risk evaluation. The results are shown in Table 5.2.

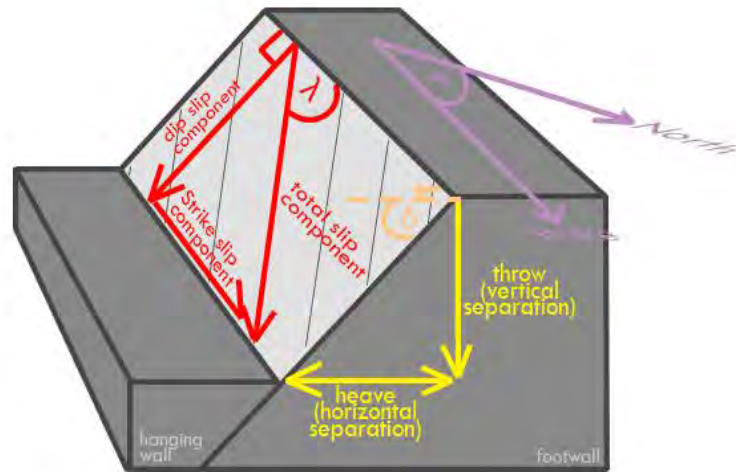


Figure 5.8. Fault geometry model. Note: ϕ = strike, δ = dip angle, and λ = slip rake (modified from Maher, 2017).

Table 5.2. Average vertical seafloor displacement of each interplate sub-region. Note: Negative VS indicates hanging wall moving down, Positive VS indicates hanging wall moving up.

Sub-region	Faulting type	Rake (λ)	Dip angle (δ)	Vertical displacement (VS: m)
S1. Offshore Sumatra-Java	Reversed	87.7	19.3	0.37
S3. Offshore Java	Normal	-98.5	40.6	-0.73
S4. Bali-Sumba	Reversed	110.9	24	0.42
S5. Flores Sea	Reversed	110.2	32.5	0.56
S6. Timor-Kai	Reversed	134.6	37.3	0.49
S7. South Banda Sea	Strike-slip	4.8	79.8	0.09
S8. Buru-Seram	Reversed	56.6	36.3	0.56
S9. Seram Sea	Strike-slip	157.4	70.0	0.41
S10. Offshore West Papua	Reversed	63.6	31.4	0.53
S12. Aru	Normal	-105.5	36.6	-0.65

According to Geist (1998), displacement of ocean surface mimics the vertical component of the rupture if the lateral dimensions for the rupture are three to four times the water depth. Because this is most often the case for significant tsunamis, it can be assumed that the initial height of tsunami is equal to vertical surface displacement.

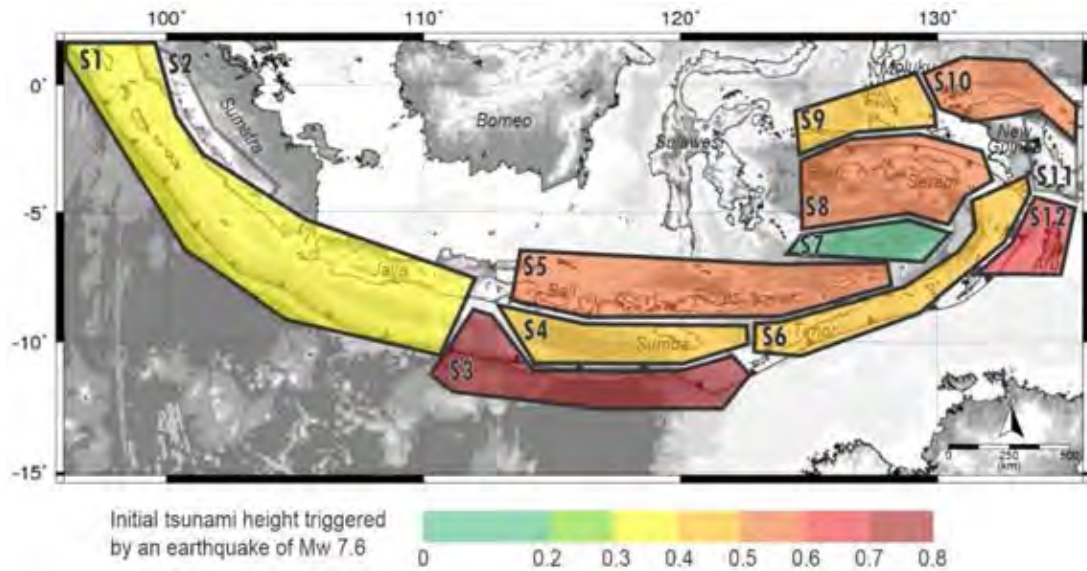


Figure 5.9. Initial height of tsunami along the Indonesian Archipelago.

From the results (Figure 5.9), both normal faulting dominated regions (S3: Java-Sumba outer rise, and S12: Aru trough) have high potentials for causing large initial tsunami (0.65-0.73 m). This could be because of steep dipping faults and almost pure normal faulting which lead to large vertical displacement. South Banda Sea (S7) has lowest potential (0.09 m) as the area is dominated by pure strike-slip faults, while Seram Sea region (S9), which is also characterized as strike-slip faulting region, has potential to trigger 0.41 m high initial tsunami. The initial heights along the SSZ increasing from 0.37 m in the west to 0.56 m in the east in accordance with increasing dip angle along the SSZ. However, these heights are of initially triggered tsunami not the tsunami height when the waves hit the shores.

5.2. Intraslab Earthquakes

Intraslab earthquakes are earthquakes occurring in a subducting slab. In this study, the earthquakes that occurred at the depth of greater than 50 km were considered as interplate earthquakes. The area then was divided into 5 sub-regions, and average FMSs for each sub-region were evaluated.

5.2.1. Focal mechanism solutions of intraslab earthquakes

Unlike interplate earthquakes, the fault plane solutions of intraslab earthquakes do not show one plane that parallels to the seismic zone. Instead, two nodal planes intersect the plane defined by the inclined seismic zone at about 45° .

Hence, it is better to use fault plane solution to define P- and P- axis, as these axes usually parallel to the dip of the slab (Molnar, 2015). The P-axis and T-axis of each sub-region is shown in Table 5.3.

Table 5.3. P- and T-axis orientation of each average FMS of intraslab earthquakes.

Sub-region	P-axis	P-axis	T-axis	T-axis
	trend	plunge	trend	plunge
D1. Sumatra-Sumbawa	194.2	27.9	35.9	71.0
D2. Java Sea	251.7	82.8	9.9	48.8
D3. Sumba-Flores-Timor	114.1	58.4	314.7	30.0
D4. Banda Sea	37.0	66.8	147.2	8.4
D5. Banda Arc	014.6	0.6	283.7	55.4

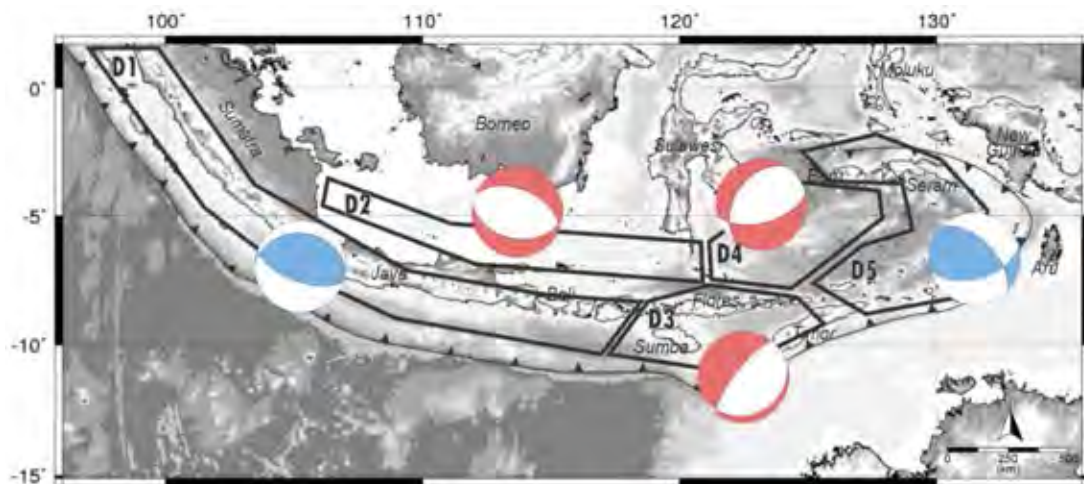


Figure 5.10. Map showing an average focal mechanism of each intraplate sub-region. Faulting mechanisms are represented in different colors, red = normal faulting, blue = reversed faulting.

5.2.2. Seismotectonic models of subducting slabs

Earthquakes in subducting slabs occur in cold interior of descending slabs. The general model of intraslab earthquakes show 2 distinct stress regimes, down-dip extension at intermediate depths (70-300 km) and down-dip compression at the depths below 300 km as shown in Figure 5.11 (Stein and Wysession, 2003). The slab extension at intermediate depths is caused by ‘slab pull’ force from the sinking

(negative buoyancy) of the cold and dense slab, while the change of mantle viscosity at the lower depth is responsible for down-dip compression.

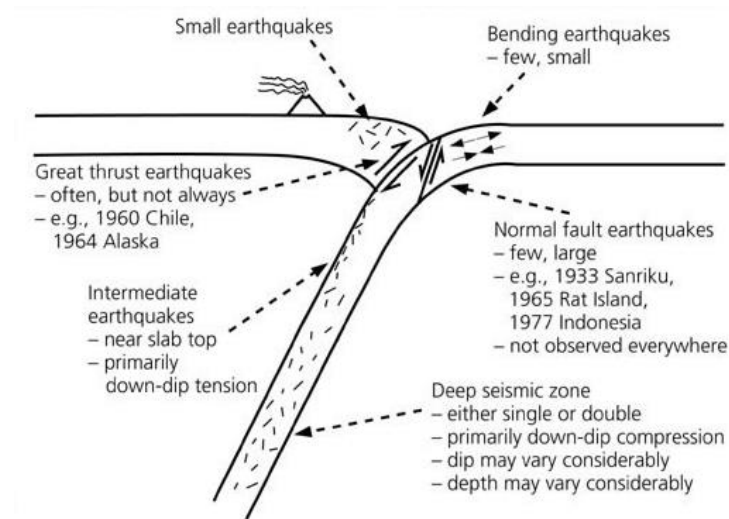


Figure 5.11. Earthquakes observed at subduction zones (Stein and Wysession, 2003).

Isacks and Molnar (1971) studied the stress distributions in the subducting lithosphere globally, using 18 focal mechanism, and found that the Sumatra slab is extended downward. Java slab shows neither down-dip compression nor extension at intermediate depth while it is compressed at the depth below 500 km (Figure 5.). With much more number of data used in this study, more detailed stress distributions were determined. The stress model in Java slab and Sumatra slab in this study are as same as the model Isacks and Molnar (1971) produced. For the Flores slab, Isacks and Molnar (1971) did not determine the stress state at the intermediate depths because the lack of data. However, Isacks and Molnar (1971) only described the down-dip stress axes, the orientation of other stress axes, whether into-slab or along-strike, were not stated.

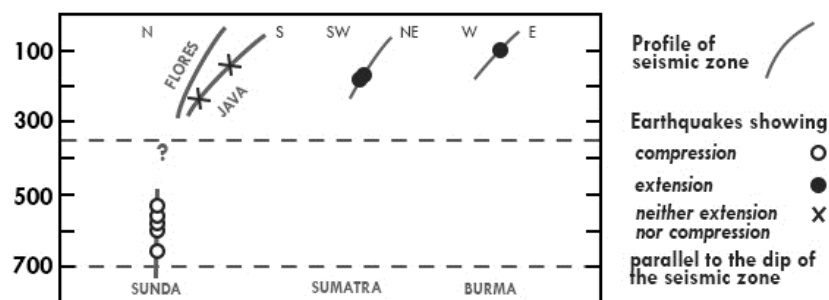


Figure 5.12. Examples of cross sections of seismicity across different subduction zones (Isacks and Molnar, 1971).

In order to study more detailed stress distribution in the subducting slab along the Indonesian Archipelago, Sumatra, Java, Flores, and Banda slabs were chosen (Figure 5.13). Then the focal mechanisms were projected onto the slab plane to determine the orientation of the P- and T- axis. The slab models used were obtained from Hayes et al. (2010) for Sumatra-Java-Flores slabs and from Pownall and Hall (2014) for Banda Arc slab.

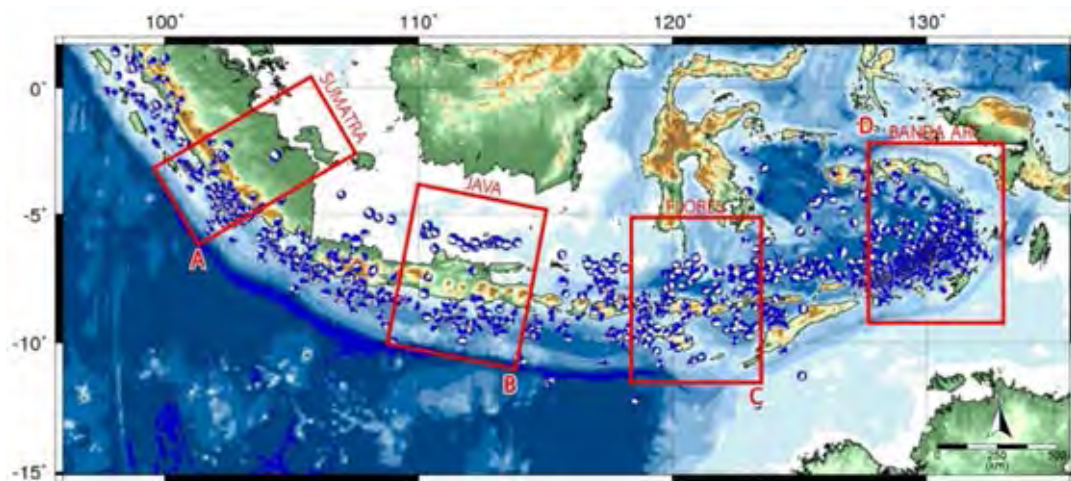


Figure 5.13. Map showing the location of (A) Sumatra slab (B) Java slab (C) Flores slab (D) Banda Arc slab.

The seismicity in the Sumatra slab extends to the depth of 250 km which in accordance to the slab model of Hayes et al. (2010). The focal mechanisms show near vertical T-axis and slightly into-slab P-axis at shallower depths (less than 65 km) and down-dip T-axis at deeper depths (Figure 5.14). Most of the down-dip tension focal mechanisms have along-strike extension. The general stress orientation in Sumatra slab agrees with the study of Isacks and Molnar (1971) and Stein and Wysession (2003).

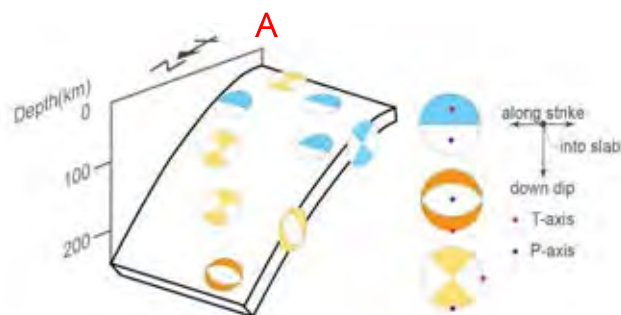


Figure 5.14. 3D seismotectonic model of the Sumatra slab.

The seismicity in Java section shows the seismic gap, where there is no earthquake between the depth of 250-500 km (Figure 5.15). The gap is growing larger westwards. The stress in the Java slab at intermediate depth is mixed between compression and extension, whereas it is predominantly down-dip compression below the seismic gap. The stress states in the slab is caused by the complexity and heterogeneity of the subducting slab, mantle convection, and the rate of subduction (Isacks, 2015). The chaotic stress orientation at the intermediate depths in the Java slab was also recognized by Isacks and Molnar (1971), Chen et al. (2004), and Alpert et al. (2010). However, the exact cause of this phenomenon is yet still unknown.

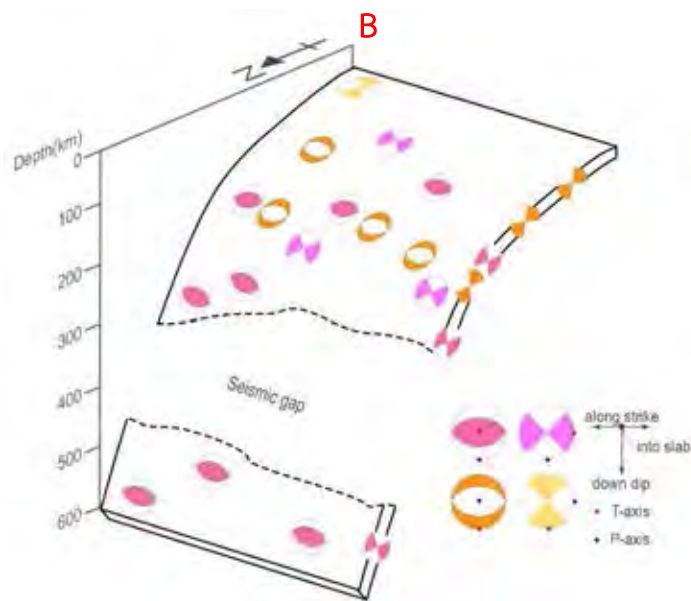


Figure 5.15. 3D seismotectonic model of the Java slab.

There is also a seismic gap in Flores slab, starting at the depths of 240-350 km to 420-530 km (Figure 5.16). The intermediate seismic zone shows 3 sections along the slab strike, down-dip tension at the eastern and the western sections and down-dip compression at the central section. The slab below the seismic gap is all compressed. The stress anomaly in Flores slab at intermediate depths could be the result of differences in slab properties as Sumba-Flores-Timor region is located at boundary between the subduction of the Indian plate to the west and the collision of Australian plate to the east. According to Stagg (1978), Scott Plateau, sub-marine plateau SE of Sumba, is defined as a transitional zone where the Indian oceanic plate gradually change to the Australian continental plate (Figure 5.17). The crust at the transitional

zone has density between those of oceanic plate and continental plate. As the lighter plate subducts, the 'slab pull' force is decreased due to decreasing weight of the subducting slab which leads to down-dip compression at intermediate depth. The extent of the Scott Plateau conforms with the extent of the compressed central Flores slab (Figure 5.17); hence, it can be interpreted that the cause of this anomaly is the differences in the slab composition.

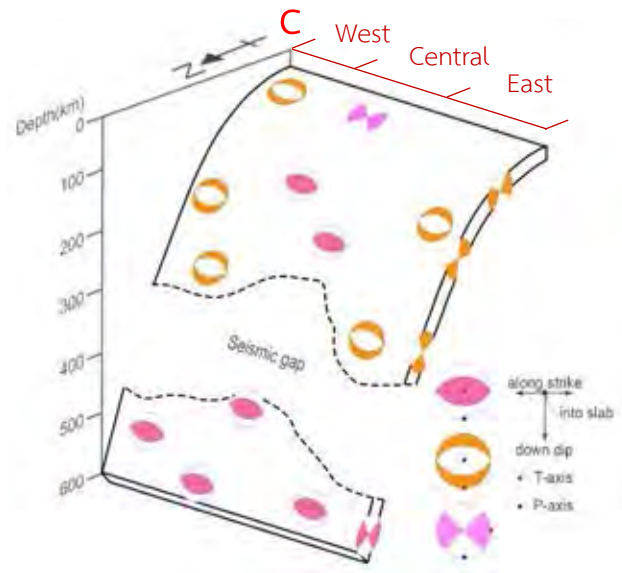


Figure 5.16. 3D seismotectonic model of the Flores slab.



Figure 5.17. Map showing the transitional zone between Indian oceanic plate and Australian continental plate (modified from Stagg, 1978).

The Banda Arc has a complex structure; it tightly curves and comprises of 2 limbs; southern and northern limbs. The seismicity is much greater in the southern limb than northern limb. In both limbs, the slab is extended downwards at intermediate depth and compressed down-dip below 250 km (Figure 5.18). At the depths of 50-180 km around where the two limbs meet, along-strike P-axis with into-slab T-axis orientation can be observed. This stress orientation indicates the synformal buckling of the slab because N-axes are parallel to the fold hinge and the T-axes is normal to the slabs.

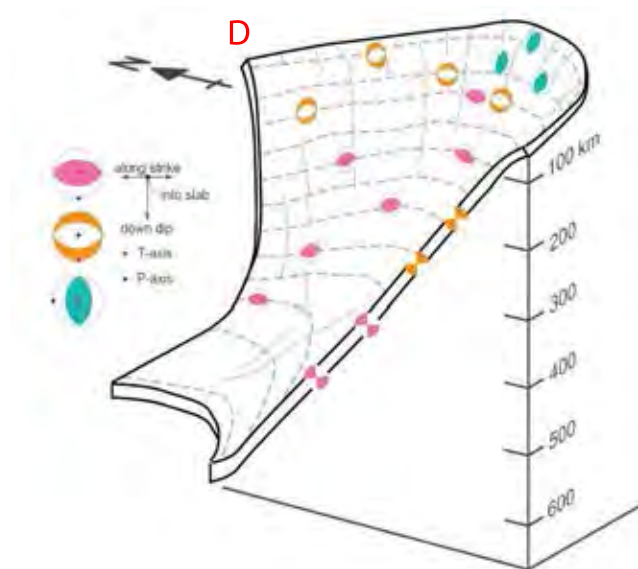


Figure 5.18. 3D seismotectonic model of the Banda Arc slab.

5.3. Conclusion

For interplate earthquakes (focal depths less than 50 km), a new seismogenic fault zone has been found in the South Banda Sea region. From the consistency of the earthquake epicenter locations, FMS, and surface lineament structures, this fault zone is proposed as a NE-SW left-lateral strike-slip faults.

Moreover, the tsunami generation potential along the Indonesian Archipelago has been evaluated. The results show that, in an event of Mw 7.6 earthquake, the Java-Simba Outer-rise and Aru Trough are capable of producing high tsunamis with initial heights of 0.65-0.73 m, while South Banda Sea area have the lowest potential.

For intraslab earthquakes (focal depths more than 50 km), the stress states in the subducting slabs were studied. Generally, the slabs are extended at intermediate

depths (50-300 km) and compressed at deeper depths (300-700 km) with some exceptions found in Java and Flores slabs. For Java slab, the stress orientation cannot be classified as it is mixed between P- and T-axes. The Flores slab shows down-dip extension at the west and east, and down-dip compression at the center. This anomalous stress orientation is resulted from the decreasing negative buoyancy as the subducting slab changes from oceanic to continental crust.

5.4. Recommendation

Further study should be conducted along the proposed seismogenic fault zone in the South Banda Sea for better understanding in its mechanism, behavior and possible seismic hazards in the area and vicinity.

Moreover, the tsunami generation potential evaluated in this study could be used to improve the tsunami warning criteria, as the tsunami warnings are issued based on magnitude and location of an earthquake (hence 'possible tsunami'). The faulting mechanism and possible vertical seafloor displacement should be taken into account for more accurate tsunami warnings. However, only earthquake magnitude and FMS were considered in this study. The maximum earthquake magnitude, returning periods, and possibilities of earthquake occurring along the Indonesian Archipelago should be looked at for better understanding of tsunami generation potential along the Archipelago.

REFERENCES

- Alpert, L.A., Becker, T.W., and Bailey, I.W. 2010. Global slab deformation and centroid moment tensor constraints on viscosity. *Geochem. Geophys. Geosyst.* 11: 1-22.
- Ammon, C.J., Kanamori, H., Lay, T., and Velasco, A.A. 2006. The 17 July 2006 Java tsunami earthquake. *Geophys. Res. Lett.* 33.
- Barth, A., Reinecker, J., and Heidbach, O. 2008. *Stress derivation from earthquake focal mechanisms*. [Online]. Available from: http://dc-app3-14.gfz-potsdam.de/pub/guidelines/WSM_analysis_guideline_focal_mechanisms.pdf.
- Charusiri, P., and Pailoplee, S. 2015. Investigations of Tsunamogenic Sources in Mainland Southeast Asia: Implication from Seismicity. *Unisearch J.* 2(1): 9-12.
- Chen, P.-F., Bina, C.R., and Okal, E.A. 2004. A global survey of stress orientations in subducting slabs as revealed by intermediate-depth earthquakes. *Geophys. J. Int.* 159: 721-733.
- Dai, C. 2015. *Source parameters inversion for recent large undersea earthquakes from GRACE data*. Doctoral dissertation. Division of Geodetic Science, School of Earth Science, The Ohio State University.
- Dongeng, N. 2009. *Manokwari Earthquake in January 2009 leaving a puzzle-unique Sorong Fault*. [Online]. Available from: <https://geologi.co.id/2009/01/15/gempa-manokwari-sesar-sorong-yang-unik/>.
- Doust, H., and Lijmbach, G. 1997. Charge constraints on the hydrocarbon habitat and development of hydrocarbons systems in Southeast Asia Tertiary Basins. In *Proc., International Conference on Petroleum Systems of SE Asia and Australasia*, pp. 115-125. Jakarta: Indonesian Petroleum Association.
- Dziewonski, A.M., Chou, T.-A., and Woodhouse, J.H. 1981. Determination of earthquake source parameters from waveform data for studies of global and source parameters from waveform data for studies of global and regional seismicity. *J. Geophys. Res.* 86: 2825-2852.
- Earthquake Research Committee. 2005. *National Seismic Hazard Maps for Japan (2005)*. Tokyo: Headquarters for Earthquake Research Promotion.

- Earthquake Research Committee. 2011. *The Focal Mechanism Solution from Initial-Motion Data, Earthquake in Hamadori, Fukushima Prefecture on April 11, 2011*. Tokyo: Headquarters for Earthquake Research Promotion.
- Elström, G., Nettles, M., and Dziewonski, A.M. 2012. The global CMT project 2004-2010: Centroid-moment tensors for 13,017 earthquakes. *Phys. Earth Planet. Inter.* 200-201: 1-9.
- Ely, K.S., and Sandiford, M. 2010. Seismic response to slab rupture and variation in lithospheric structure beneath the Savu Sea, Indonesia. *Tectonophysics.* 483: 112-124.
- Fernández-Blanco, D., Philippon, M., and von Hagke, C. 2016. Structure and kinematics of the Sumatran Fault System in North Sumatra (Indonesia). *Tectonophysics.* 963(B): 453-464.
- Geist, E.L. 1998. Local tsunamis and earthquake source parameters. *Adv. Geophys.* 39: 117-209.
- Goes, S., Agrusta, R., van Hunen, J., and Garel, F. 2017. Subduction-transition zone interaction: A review. *Geosphere.* 13(3): 644-664.
- Grotzinger, J., Jordan, T., Press, F., and Siever, R. 2007. Earthquakes. In *Understanding Earth*. 5th ed. New York, NY: W. H. Freeman and Company.
- Hall, R., Patria, A., Adhitama, R., Pownall, J.M., and White, L. 2017. Seram, The Seram Trough, The Aru Trough, The Tanimbar Trough and The Weber Deep: A New Look at Major Structures in The Eastern Banda Arc. *Proc., the Indonesian Petroleum Association 41st Annual Convention & Exhibition, May 2017, IPA17-91-G*. Jakarta: Indonesian Petroleum Association.
- Hamilton, W. 1974. Earthquake map of the Indonesian region. *USGS Misc. Invest. Ser. Map I-875C*.
- Hamilton, W. 1979. Tectonics of the Indonesian Region. *U.S. Geol. Surv. Prof. Pap.* 1078: 345.
- Hanks, T. C., and Kanamori, H. 1979. A moment magnitude scale. *J. Geophys. Res.* 84: 2348-2350.
- Hauksson, E. 1990. Earthquakes, faulting, and stress in the Los Angeles basin. *J. Geophys. Res.* 95: 15365-15394.

- Hayes. G.P., Wald, D.J., and Johnson, R.L. 2012. Slab 1.0: A three-dimensional model of global subduction zone geometries. *J. Geophys. Res.* 117:148-227.
- Hill, E.M., Borrero, J.C., Huang, Z., Qiu, Q., Banerjee, P., Natawidjaja, D.H., Elosegui, P., Fritz, H.M., Suwargadi, B.W., Pranantyo, I.R., Li, L., Macpherson, K.A., Skanavis, V., Synolakis, C.E., and Sieh, K. 2012. The 2010 Mw 7.8 Mentawai earthquake: Very shallow source of a rare tsunami earthquake determined from tsunami field survey and near-field GPS data. *J. Geophys. Res.* 117: 2156-2202.
- Isacks, B., and Molnar, P. 1971. Distribution of stresses in the descending lithosphere from a global survey of focal-mechanism solutions of mantle earthquakes. *Rev. Geophys.* 9(1): 103-174.
- Janephanut, P. 2015. *Seismicity rate change along the Indonesian Islands*. Senior's project. Department of Geology, Faculty of Science, Chulalongkorn University.
- Japan Nuclear Fuel Limited. n.d. *Safety: Geological survey (on the ground)*. [Online]. Available: <https://www.jnfl.co.jp/en/activity/safety/>.
- Khatti, K. 1973. Earthquake focal mechanism studies – A review. *Earth Sci. Rev.* 9(1): 19-63.
- Ketthong, T. 2016. *Investigation of focal mechanism and fractal dimension along the Sumatra-Andaman Subduction Zone*. Master's thesis. Department of Geology, Faculty of Science, Chulalongkorn University.
- Kisslinger, C., Bowman, J.R., and Koch, K. 1982. Determination of focal mechanism from SV/P amplitude ratios at small distances. *Phys. Earth Planet In.* 30: 172-176.
- Krabbenhoft, A., Weinrebe, R.W., Kopp, H., Flueh, E.R., Ladage, S., Papenberg, C., Planert, L., and Djajadihardja, Y. 2010. Bathymetry of the Indonesian Sunda margin-relating morphological features of the upper plate slopes to the location and extent of the seismogenic zone. *Nat. Hazards Earth Syst. Sci.* 10: 1899-1911.
- Lay, T. 2016. Great Earthquakes on Plate Boundaries. *Oxford Research Encyclopedia of Natural Hazard Science*. Oxford: Oxford University Press.
- Levin, B.W., and Nosov, M.A. 2014. Source of a tsunami of seismotectonic origin. In *Physics of Tsunamis*. pp.35-88. Basel: Springer International Publishing.
- Maher, H.D., Jr. 2017. *Description of faults*. [Online]. Available from: <http://maps.unomaha.edu/Maher/GEOL3300/week2/fault.html>

- McCaffrey, R. 2009. The Tectonic Framework of Sumatran Subduction Zone. *Annu. Rev. Earth Planet. Sci.* 37: 345–366.
- Michael, A.J. 1984. Determination of stress from slip data: Faults and folds. *J. Geophys. Res.* 89: 517-526.
- Michael, A.J. 1987. Use of focal mechanisms to determine stress: A control study. *J. Geophys. Res.* 92: 357-368.
- Molnar, P. 2015. Subduction of oceanic lithosphere. In *Plate Tectonics: A very short introduction*. pp. 53-76. Oxford: Oxford University Press.
- Myhill, R. 2013. Slab buckling and its effect on the distributions and focal mechanisms of deep-focus earthquakes. *Geophys. J. Int.* 192: 837-853.
- Murotani, S., Satake, K., and Fujii, Y. 2013. Scaling relations of seismic moment, rupture area, average slip, and asperity size for M~9 subduction-zone earthquakes. *Geophys. Res. Lett.* 40: 5070-5074.
- Noda, A. 2013. Strike-Slip basin: Its configuration and sedimentary facies. In *Mechanism of Sedimentary Basin Formation - Multidisciplinary Approach on Active Plate Margins*. pp. 27-57. London: InTech.
- Norton, M. 2008. *Focal mechanism*. [Online]. Available from: https://en.wikipedia.org/wiki/Focal_mechanism.
- Pailoplee, S. 2017. Earthquake activities along the Indonesian Sunda Margin: a seismicity approach. *Geoscience J.* 24: 535-541.
- Pailoplee, S. 2018. Earthquake sources in ASEAN. In *Statistical Seismology*. pp. 1-24. Bangkok: Department of Geology, Chulalongkorn University.
- Pownall, J.M., and Hall, R. 2014. Neogene extension on Seram: A new tectonic model for the Northern Banda Arc. *Proc., Indonesian Petroleum Association 38th Annual Convention & Exhibition, May 2014*, IPA14-G-305. Jakarta: Indonesian Petroleum Association.
- Sandiford, M. 2008. Seismic moment release during slab rupture beneath the Banda Sea. *Geophys. J. Int.* 174:659-671.
- Seismology Research Center. n.d. *Earthquake size*. [Online]. Available from: <http://www.src.com.au/earthquake-size/>.
- Shah, S.T. 2015. *Stress tensor inversion from focal mechanism solutions and earthquake probability analysis of Western Anatolia, Turkey*. Master's thesis.

Department of Geological Engineering, Graduate School of Natural and Applied Sciences, Middle East Technical University.

- Shulgin, A. 2012. *Subduction zone segmentation, Indonesia*. Doctoral dissertation. Kiel University.
- Simons, W. J. F., Socquet, A., Vigny, C., Ambrosius, B.A.C., Abu, S.H., Promthong, C., Subarya, C., Sarsito, D.A., Matheussen, S., Morgan, P., and Spakman, W. 2007. A decade of GPS in Southeast Asia: Resolving Sundaland motion and boundaries. *J. Geophys. Res.* 112: 2156-2202.
- Spakman, W., and Hall, R. 2010. Surface deformation and slab–mantle interaction during Banda arc subduction rollback. *Nature Geoscience.* 3: 562-566.
- Stagg, H.M.J. 1978. The geology and evolution of the Scott Plateau. *APEA Journal.* 18: 34–43.
- Stanley, C.E., and Harris, R. 2009. Tectonic evolution of forearc nappes of the active Banda arc-continent collision: Origin, age, metamorphic history and structure of the Lolotoi Complex, East Timor. *Tectonophysics.* 479: 66-94.
- Stein, S., and Wysession, M. 2003. Earthquake. In *An Introduction to Seismology, Earthquakes, and Earth Structure.* pp. 215-251. Malden, MA: Blackwell Publishing.
- Vajchakorn, K. 2016. *Investigation of focal mechanism and fractal dimension in the Thailand-Laos-Myanmar Borders.* Master's thesis. Department of Geology, Faculty of Science, Chulalongkorn University.
- U.S. Geological Survey. 1996. *Focal Mechanisms.* [online]. Available from: <https://earthquake.usgs.gov/learn/topics/beachball.php>.
- U.S. Geological Survey. 2016. *What it is about an earthquake that causes tsunami?* [online]. Available from: https://www.usgs.gov/faqs/what-it-about-earthquake-causes-a-tsunami?qt-news_science_products=7#qt-news_science_products.
- Watkinson, I.M., and Hall, R. Fault systems of the eastern Indonesian triple junction: evaluation of Quaternary activity and implications for seismic hazards. *Geol. Soc. Spec. Publ.* 441: 71-120.